

## RESEARCH ARTICLE

# Oxidation of the 1-naphthyl radical $C_{10}H_7\cdot$ with oxygen: Thermochemistry, kinetics, and possible reaction pathways

 Nadia Sebbar  | Henning Bockhorn | Dimosthenis Trimis

 KIT- Karlsruhe Institute of Technology,  
 Engler-Bunte-Institut,  
 Verbrennungstechnik, Karlsruhe,  
 Germany
**Correspondence**
 Nadia Sebbar, KIT- Karlsruhe Institute of  
 Technology, Engler-Bunte-Institut,  
 Verbrennungstechnik, Engler-Bunte Ring  
 7, D-76131 Karlsruhe, Germany.  
 Email: [nadia.sebbar@kit.edu](mailto:nadia.sebbar@kit.edu)
**Abstract**

The reaction of the 1-naphthyl radical  $C_{10}H_7\cdot$  ( $A2\cdot$ ) with molecular ( $^3O_2$ ) and atomic oxygen, as part of the oxidation reactions of naphthalene, is examined using ab-initio and DFT quantum chemistry calculations. The study focuses on pathways that produce the intermediate final products CO, phenyl and  $C_2H_2$ , which may constitute a repetitive reaction sequence for the successive diminution of six-membered rings also in larger polycyclic aromatic hydrocarbons. The primary attack of  $^3O_2$  on the 1-naphthyl radical leads to a peroxy radical  $C_{10}H_7OO\cdot$  ( $A2OO\cdot$ ), which undergoes further propagation and/or chain branching reactions. The thermochemistry of intermediates and transition state structures is investigated as well as the identification of all plausible reaction pathways for the  $A2\cdot + O_2 / A2\cdot + O$  systems. Structures and enthalpies of formation for the involved species are reported along with transition state barriers and reaction pathways. Standard enthalpies of formation are calculated using ab initio (CBS-QB3) and DFT calculations (B3LYP, M06, APFD). The reaction of  $A2\cdot$  with  $^3O_2$  opens six main consecutive reaction channels with new ones not currently considered in oxidation mechanisms. The reaction paths comprise important exothermic chain branching reactions and the formation of unsaturated oxygenated hydrocarbon intermediates. The primary attack of  $^3O_2$  at the  $A2\cdot$  radical has a well depth of some  $50 \text{ kcal mol}^{-1}$  while the six consecutive channels exhibit energy barriers below the energy of the  $A2\cdot$  radical. The kinetic parameters of each path are determined using chemical activation analysis based on the canonical transition state theory calculations. The investigated reactions could serve as part of a comprehensive mechanism for the oxidation of naphthalene. The principal result from this study is that the consecutive reactions of the  $A2\cdot$  radical, viz. the channels conducting to a phenyl radical  $C_6H_5\cdot$ ,  $CO_2$ , CO (which oxidized to  $CO_2$ ) and  $C_2H_2$  are by orders of magnitude faster than the activation of naphthalene by oxygen ( $A2 + O_2 \rightarrow A2\cdot + HO_2$ ).

**KEYWORDS**

ab-initio, DFT, kinetics, naphthyl, oxidation

This is an open access article under the terms of the [Creative Commons Attribution-NonCommercial-NoDerivs](https://creativecommons.org/licenses/by-nc-nd/4.0/) License, which permits use and distribution in any medium, provided the original work is properly cited, the use is non-commercial and no modifications or adaptations are made.

© 2023 The Authors. *International Journal of Chemical Kinetics* published by Wiley Periodicals LLC.

## 1 | INTRODUCTION

It is well accepted that one essential pathway for the growth of polycyclic aromatic hydrocarbons (PAH) during fuel rich (sooting) combustion comprises a repetitive H-abstraction- $C_2H_2$ -addition and subsequent formation of six-membered rings, the so-called HACA mechanism.<sup>1,2</sup> We hypothesize that similar repetitive reaction sequences are taking place during the oxidation/decomposition of large PAHs being present in soot particles or forming the basic structural graphene-like units stacked in primary soot particles, respectively. The assumption is that the oxidation may follow a repetitive reaction sequence through the mass loss via  $C_2H_2$  and CO, resulting in the successive diminution of a six-membered ring. This reaction scheme, exemplified with the coronyl-radical is schematically illustrated in Figure 1.

The first steps of the oxidation of aromatic hydrocarbons and their radicals with different numbers of rings as occurring in the reaction sequence given in Figure 1 by molecular oxygen ( $^3O_2$ ) has been examined in a previous study.<sup>3</sup> The results point to similarities in the oxidation behavior of different PAHs supporting the above hypothesis. Continuing the work carried out in,<sup>3</sup> the detailed reaction pathways for the oxidation of the 1-naphthyl-radical, which is the last but one species in the reaction sequence, by oxygen ( $^3O_2$  and O) are investigated in this study with the help of computational methods. Similar investigations on larger aromatics will be reported in separate studies in preparation. The oxidation of the phenyl-radical has been presented in refs.<sup>4,5</sup>

The formation and oxidation of naphthalene has been addressed in various studies. Mebel et al.<sup>6</sup> investigated experimentally and via quantum chemistry calculations the formation of naphthalene by the growth of smaller molecules or radicals such as benzene, phenyl, cyclopentadienyl, and so on. With the help of ab initio calculations, Chu et al.<sup>7</sup> developed and proposed a pressure-dependent reaction mechanism describing the HACA chemistry for both 1- and 2-naphthyl radicals ( $1-C_{10}H_7$  and  $2-C_{10}H_7$ ) including  $C_{12}H_9$ ,  $C_{14}H_9$ , and  $C_{14}H_{11}$  potential energy surfaces over a wide range of temperature and pressure conditions and tried to explain the unexpected experimen-

tal results of Parker et al.<sup>8</sup> Comandini et al.<sup>9</sup> studied the energy surfaces for the radical/ $\pi$ -bond addition reactions between different single-ring aromatic hydrocarbons. Concerning naphthalene oxidation, only little data is available. In several studies,<sup>10–14</sup> the focus is on the investigation of reactions of naphthalene and/or naphthyl with the hydroxyl radical OH. Some studies report the reaction of naphthyl with  $O_2$ .<sup>15–17</sup> These studies put weight on the primary reactions but not on details of the degradation of the first aromatic ring. Zhou et al.<sup>18</sup> investigated potential energy surfaces (PESs) of the reactions of 1- and 2-naphthyl radicals with molecular oxygen. Their calculations show the expected barrier-free formation of naphthylperoxy radicals. The subsequent reaction steps of the chemically activated 1- and 2- $C_{10}H_7OO\cdot$  ( $A2OO\cdot$ ) peroxy radicals investigated in Ref. 18 are the elimination of an oxygen atom leading to the formation of 1- and 2-naphthoxy radicals, respectively. These can undergo unimolecular decomposition producing an indenyl radical + CO. Additionally, they investigated the ipso addition of the oxygen atom to the ring leading to bicyclic intermediates which then decompose to  $C_9H_7$  (indenyl) +  $CO_2$ ,  $1,2-C_{10}H_6O_2$  (1,2-naphthoquinone) + H, and  $1-C_9H_7O$  (1-benzopyranil) + CO. Kislov et al.<sup>19</sup> reported about the O–O scission in  $A1OO\cdot$  and  $A2OO\cdot$  to phenoxy and naphthoxy radicals. They state that the general trends in the oxidation kinetics of phenyl and naphthyl radicals are similar.

In the present study, a detailed mechanistic investigation of the oxidation of the 1-naphthyl radical by  $^3O_2$  and O is performed with focus on the main reaction pathways of the degradation of the first aromatic ring leading to phenyl, acetylene,  $CO_2$  and CO.

## 2 | COMPUTATIONAL METHODS

### 2.1 | Quantum chemistry calculations – ab-initio and density functional methods

Molecular properties of the species involved in the  $A2 + O_2 / A2 + O$  and  $A2\cdot + O_2 / A2\cdot + O$  systems are determined using the Gaussian 16<sup>20,21</sup> program suite. DFT methods, viz. M06,<sup>22,23</sup> the newly developed APFD<sup>24</sup> and

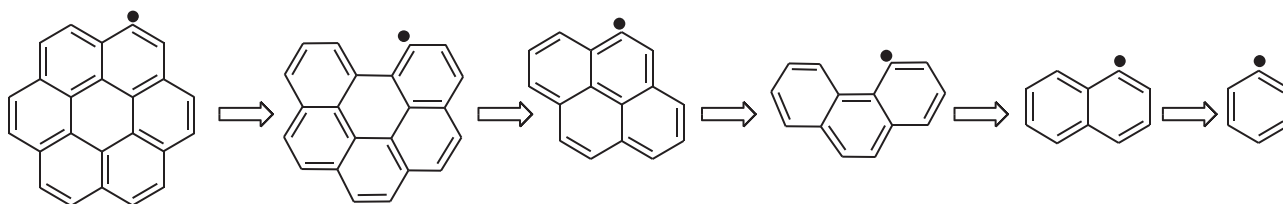


FIGURE 1 Hypothetical reaction sequence for the oxidation of coronene.

the B3LYP<sup>25–27</sup> are used for the calculations along with the CBS-QB3<sup>28,29</sup> ab-initio method. Structural parameters for all molecules are optimized using B3LYP, M06 and APFD with 6-311G(d,p) basis set. Harmonic vibration frequencies and zero-point vibrational energies (ZPVE) are computed at the same level. The optimized geometry parameters are used to obtain total electronic energies.<sup>25–27</sup> The 6-311G(d,p) set is chosen because it has a comparatively large basis set and it is still reasonable for structure optimization and force constant calculations of the molecules in this study. The B3LYP/6-311G(d,p) method has been tested in several studies. For example, Mebel et al.<sup>30</sup> have shown that the B3LYP/6-311G(d,p) method gives similar energies compared to those obtained at higher level calculations (G2M(RCC,MP2)) for a number of unsaturated peroxy species, where the final total energies obtained from G2 theory are effectively at the QCISD(T)/6-311+G(3df,2p) level. Peterson et al.<sup>31</sup> have recommended the use of B3LYP for geometry and frequencies in several CBS calculations. The density function calculated geometries are often selected and serve as an accurate structure for higher-level composite method calculations.

In this work, special focus is given to the APFD method because of comparable accuracy as B3LYP or M06. This is probably due to the developed function to avoid the spurious long-range attractive or repulsive interactions that are found in most density functional theory (DFT) models. Austin et al.<sup>24</sup> report that this method provides a sound baseline for the addition of an empirical dispersion correction term, which is developed from a spherical atom model (SAM). They found that the accuracy of APFD is comparable to that of B2PLYP-D3 and CCSD(T), when the aug-cc-pVTZ basis is used, however at much lower computational cost. The results from APFD are used in this study, because, APFD has been improved and is more accurate compared to the previous DFT methods. Further, APFD can handle large molecules, and by using a single method, the errors in the calculations due to the method are the same for all compounds.

The present study considers a two-ring system and is part of a series of future calculations in which the number of rings will be increased gradually towards larger polycyclic aromatic hydrocarbons as model molecules for graphene layers, which are assembled in primary soot particles. This justifies the use of DFT methods (in particular APFD) which are, in contrast to CBS-QB3, affordable and permit handling of large molecules at low computational costs.

It has been shown that the use of a DFT method combined with isodesmic or homodesmic reactions yield reasonable accurate energies.<sup>32,33</sup> Whenever possible, the calculations in this study are based on isodesmic reactions, in which the unknown formation enthalpies of the

considered species are coupled to experimental or previously evaluated enthalpies of formation, needed in the isodesmic analysis. Transition state structures were identified by their single imaginary frequency, whose mode of vibration connects the reactant and the product.

The entropies and heat capacities for the compounds (radicals and transition state structures) are based on the calculated vibration frequencies, moments of inertia, symmetry, spin degeneracy, and optical isomers. (All values are available from the authors upon request.) Frequencies and moments of inertia from the optimized APFD/6-311G(d,p) structures were used to calculate the contributions to entropy and heat capacity on the basis of formulas from statistical mechanics and by use of the SMCPS code.<sup>34</sup> Torsional frequencies are not included in the contributions to entropy and heat capacities, but are determined on each internal rotor analysis. Hindered internal rotor contributions to entropy and heat capacities are determined at B3LYP/6-31G(d,p) using the Rotator program.<sup>35</sup>

The thermodynamic properties calculated in this study are converted into the NASA polynomial format (available in the [supplementary material](#)) using THERMFIT.<sup>34</sup> With the help of ThermKin<sup>34</sup> the forward rate constants,  $k(T)$ , based on the canonical transition state theory (CTST) are determined. The developed set of reactions is listed in Table 1.

## 2.2 | Nomenclature

The nomenclature used in this work is as follows: **Y(A)** indicates a cyclic structure, **A•** or **AJ** represents a radical site on the structure, **D** indicates a double bond (CDO is C O), **TS** is a transition state structure, and, for example, **Y(C5)DO** represents a cyclic five-membered carbon atom ring with a double bond to an oxygen on a ring carbon atom. The transition state structures of the continuing reactions for each reaction path are numbered according to the respective reaction path TS1-1, TS1.1-1 ... for TS1 and consecutive paths, TS2-1, TS2.1-1 ... for TS2 and consecutive paths etc... as illustrated in Figures 4–14. The structures of the involved species and the corresponding nomenclature are illustrated in detail in Table A in the appendix.

## 3 | RESULTS AND DISCUSSION

The initial step of the oxidation of this class of molecules is through the abstraction of a C–H hydrogen through radicals such as H, OH, O, OOH, CH<sub>3</sub> present during combustion at reasonable concentration levels. For example, the abstraction reaction with OH is slightly exothermic

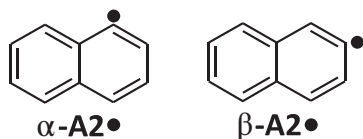


FIGURE 2 structure of A2• in  $\alpha$ - and  $\beta$ -C<sub>10</sub>H<sub>7</sub>•.

and exhibits low energy barriers in the order of 10 kcal mol<sup>-1</sup>. In non-flame conditions at temperatures in the range around 1000 K the concentration level of these radicals is very low and the H-abstraction occurs mainly by O<sub>2</sub>. The reaction C<sub>10</sub>H<sub>8</sub> + O<sub>2</sub> → C<sub>10</sub>H<sub>7</sub>• + OOH exhibits a high barrier of some 70 kcal mol<sup>-1</sup>, relative to the stable naphthalene molecule. The H-abstraction from naphthalene by O<sub>2</sub> results in radical sites, C<sub>10</sub>H<sub>7</sub>• (A2•), in  $\alpha$ - or  $\beta$ -position (see Figure 2).

Quantum chemistry calculations indicate that both radicals,  $\alpha$ -A2• (1-naphthyl) and  $\beta$ -A2• (2-naphthyl), have the same standard enthalpy of formation of ~ 97 kcal mol<sup>-1</sup>. The energy barrier for the H-abstraction by <sup>3</sup>O<sub>2</sub> estimated with ~70 kcal mol<sup>-1</sup> is similar to that for larger aromatic hydrocarbons. This has been shown for aromatic hydrocarbons containing four rings<sup>36</sup> and for a series of polycyclic species containing up to seven rings.<sup>3</sup>

Figure 3 depicts the major reaction channels of the oxidation of the 1-naphthyl radical (A2•) indicating two classes of oxidation reactions: A2• + O<sub>2</sub> and A2• + O. Almost all reactions conduct to the formation of phenyl radicals, CO and acetylene. The different reaction channels are discussed in deeper detail in the following subsections. The 1-naphthyl radical isomer is chosen for the present study, because the oxygen of the peroxy radical can interact with the adjacent ring in contrast to the 2-naphthyl radical. To verify that no important reaction channel is missing, the possible pathways of the  $\beta$ -C<sub>10</sub>H<sub>7</sub>OO• (2-naphthyl) isomer have been roughly investigated. These results reveal that the  $\beta$ -C<sub>10</sub>H<sub>7</sub>OO• isomer reacts approximately likewise to  $\alpha$ -C<sub>10</sub>H<sub>7</sub>OO• on similar energy levels and forming the same main product species as resumed in Figure A of the [supplementary material](#).

### 3.1 | Enthalpy of formation, $\Delta_f H_{298}^0$ , entropy S°(298) and heat capacities

Using the four methods mentioned in Section 2.1, enthalpies of formation of the several compounds resulting from A2• + O<sub>2</sub> and A2• + O, as well as the corresponding transition state structures are calculated. Detailed results of the calculation of the enthalpies from the four methods B3LYP, M06, and APFD with 6-311G(d,p) basis set and

the CBS-QB3 ab-initio method are listed in the [supplementary material](#), Table SM2 to SM8. Structures of the identified species are illustrated in Table A in the appendix to this paper. Equally well, the entropies S<sub>298</sub><sup>0</sup> and heat capacities Cp(T) for all radicals, intermediates and final products of the A2• + O<sub>2</sub> / A2• + O reaction system are calculated and listed in the [supplementary material](#) Table SM9.

## 3.2 | Reactions of naphthyl radical A2• (C<sub>10</sub>H<sub>7</sub>•) with O<sub>2</sub>

### 3.2.1 | Formation of a stable peroxy radical A2OO• (Channel 1)

The reaction of molecular oxygen with A2• results in a peroxy radical A2OO•. The formation of the stabilized A2OO• radical is an important intermediate reaction step occurring at low and high temperatures. Similar to reaction systems such as phenyl + O<sub>2</sub> or butanone-yl + O<sub>2</sub>,<sup>37–40</sup> it takes place without energy barrier. The formation of the chemically activated naphthyl-peroxy [A2OO•]<sup>#</sup> occurs with nearly 50 kcal mol<sup>-1</sup> excess of energy allowing six consecutive reaction channels with barriers below the energy of the initial state A2• + O<sub>2</sub>. The calculated energy for the dissociation of the naphthyl-peroxy radical (A2OO•) to naphthyl + O<sub>2</sub> in dependence on the C–OO bond distance in comparison with the corresponding bond cleavage for the phenyl-peroxy radical (C<sub>6</sub>H<sub>5</sub>OO•) is illustrated in Figure B of the supplementary material. The APFD (DFT) calculations reproduce the same energy for the two reaction systems and indicate that there is no barrier in addition to the endothermicity of the C–OO dissociation reaction. This result is also in concordance with those of Zhou et al.<sup>18</sup> and Park et al.<sup>16</sup>

The primary pathways resulting from the further reactions of the peroxy radical A2OO•, see Figure 4, include:

- Channel 1.1:** Addition of the oxygen radical to the adjacent carbon atom of the same ring via **TS1.1-1**
- Channel 1.2:** Ipso addition of the oxygen radical via **TS1.2-1**
- Channel 1.3:** Addition of the oxygen atom to adjacent carbon atom of the neighbor ring via **TS1.3-1**
- Channel 1.4a:** Hydrogen abstraction by the oxygen atom from neighbor carbon atom of the same six membered ring via **TS1.4a-1**
- Channel 1.4b:** Hydrogen abstraction by the oxygen atom from the neighboring carbon atom of the adjacent six membered ring via **TS1.4b-1**
- Channel 2:** RO–O bond cleavage via **TS2-1**.

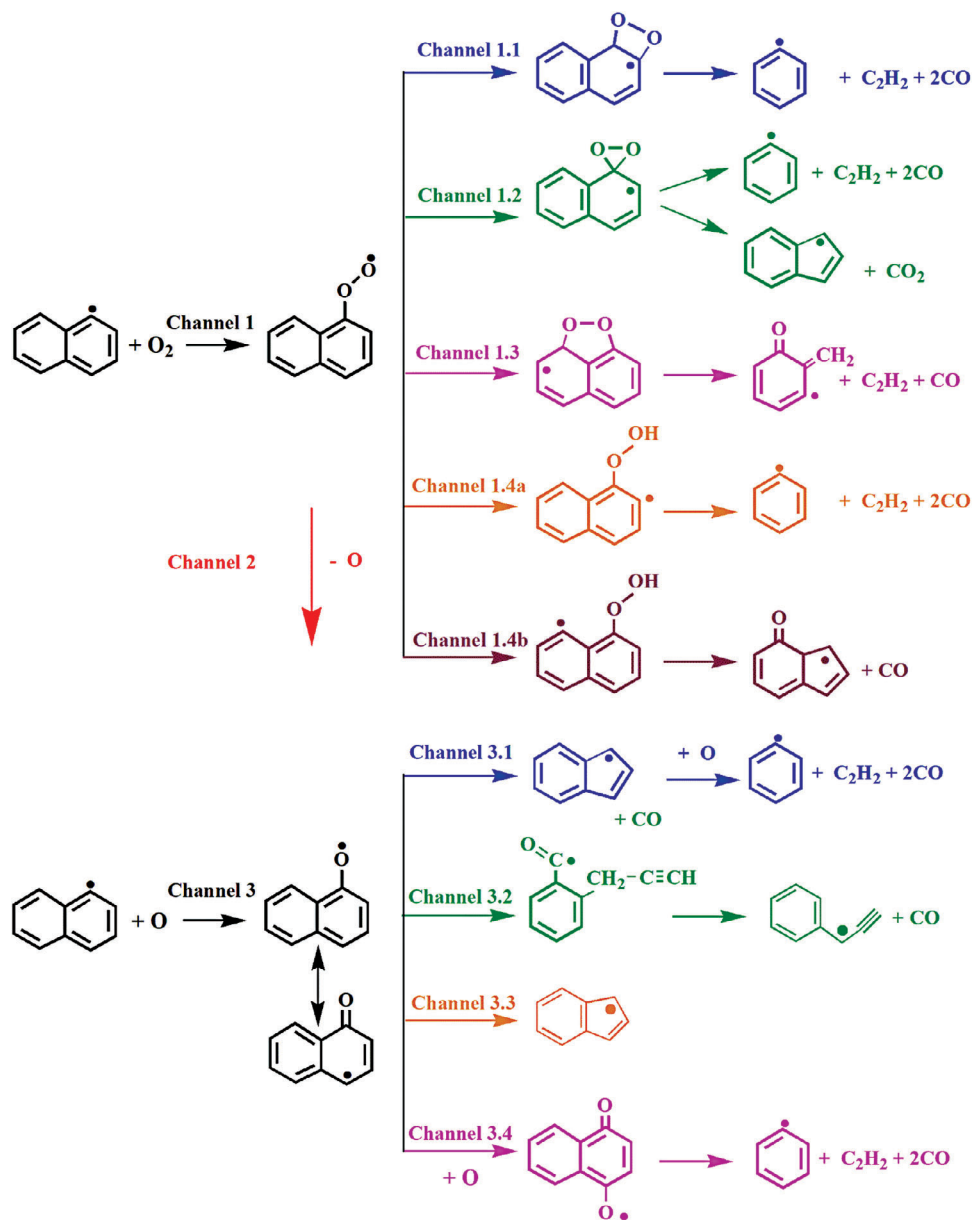


FIGURE 3 Major reaction channels for  $\alpha$ -A2• +  $O_2$  and  $\alpha$ -A2• +  $O$ .

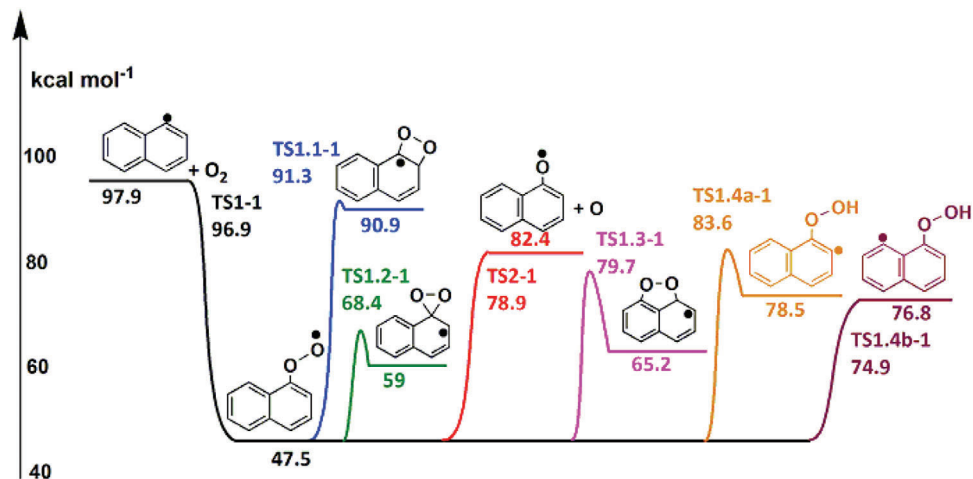


FIGURE 4 Potential diagram for primary consecutive reactions channels for A2OO• (APFD/6-311G(d,p) calculations).

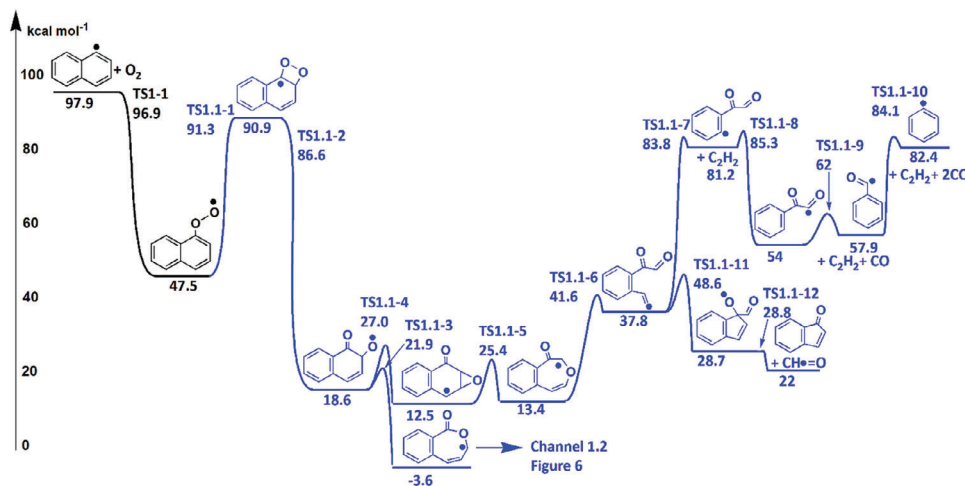


FIGURE 5 Channel 1.1: Formation and further reactions of A2•YC2O2 (APFD/6-311G(d,p) calculations).

### 3.2.2 | Formation of A2•YC2O2 through addition of the oxygen atom to the adjacent carbon atom (Channel 1.1)

The addition of the oxygen from the peroxy radical to the adjacent carbon atom of the same ring via **TS1.1-1** constitutes one of the consecutive reactions involving the peroxy radical, Channel 1.1. This reaction involves the double C = C bond opening in the phenyl ring with an additional energy of ca. 44 kcal mol<sup>-1</sup> relative to the initial peroxy A2OO• radical, see Figure 5. The reaction results in an unstable four membered ring, A2•YC2O2, at approximately 91 kcal mol<sup>-1</sup>. However, this relatively high energy level along this reaction path is still below the energy of the initial state A2• + O<sub>2</sub>. Due to the high strain inside the four-membered ring in A2•YC2O2 the weak O–O bond breaks easily via **TS1.1-2** forming a more stable radical, A2O•CDO. Due to the relative low energy of this intermediate species of 18.6 kcal mol<sup>-1</sup>, the energy release of this step amounts to 72 kcal mol<sup>-1</sup>.

The oxygen radical site in ortho-A2O•DO has two adjacent carbon atoms and consequently two alternative transformation reactions via **TS1.1-3** and **TS1.1-4** are possible. The calculations indicate a facile attack of the oxygen radical via **TS1.1-3** with only 3.3 kcal mol<sup>-1</sup> at the adjacent carbon atom followed by an intra-molecular rearrangement to a seven membered ring AIYCDOOC•CC at low energy (–3.6 kcal mol<sup>-1</sup>). Further reactions of this species are discussed and illustrated in Section 3.2.3 and Figure 6.

The other plausible reaction is the addition of the oxygen radical via **TS1.1-4** to the adjacent carbon not bonded to the oxygen. This requires some 8 kcal mol<sup>-1</sup> and forms a bicycle A2•DOYC2O at relatively low energy of 12.5 kcal mol<sup>-1</sup> (see potential diagram in Figure 5 and illustration in Table A). This energy is 34.3 kcal mol<sup>-1</sup> below

that of the peroxy radical. A2•DOYC2O rearranges via **TS1.1-5** to AIYC2OC•CDO by opening the bicycle over an energy barrier of some 13 kcal mol<sup>-1</sup>. The excess of energy gained by the system then favors further dissociation of AIYC2OC•CDO by opening the ring through **TS1.1-6** with about 28.2 kcal mol<sup>-1</sup>. A sequence of dissociation reactions with higher energy barriers follows: The elimination of C<sub>2</sub>H<sub>2</sub> takes place via a relatively high barrier of 46 kcal mol<sup>-1</sup> (**TS1.1-7**) to A1•CDOCDO. This radical species releases some energy by undergoing H-abstraction (**TS1.1-8**) to a more stable isomer A1CDOC•DO lying some 26 kcal mol<sup>-1</sup> lower. The last two reaction steps consist of two CO eliminations via **TS1.1-9** and **TS1.1-10** to a phenyl radical.

After formation of AIYCC•CDOCDO a ring closure can take place over ca. 11 kcal mol<sup>-1</sup> (**TS1.1-11**) followed by a barrierless C–C bond dissociation (**TS1.1-12**) to a stable AIYC5DO + CH = O.

### 3.2.3 | Formation of A2•YCO2 through ipso addition of the oxygen atom to the ring (Channel 1.2)

The second pathway is the addition of the oxygen in the peroxy radical via **TS1.2-1** to the ipso position (Channel 1.2). The resulting dioxirane-naphthyl radical A2•YCO2 (see Figures 6 and 7) has a bicyclic structure with a three-membered peroxy ring. It is formed via **TS1.2-1** with 68.4 kcal mol<sup>-1</sup>. This energy barrier is about 30 kcal mol<sup>-1</sup> below the A2• + O<sub>2</sub> entrance channel and only 20.9 kcal mol<sup>-1</sup> above the stabilized A2OO• radical which is in excellent agreement with the 20.7 kcal mol<sup>-1</sup> calculated at G3 level in Ref. 18 The weak peroxide bond in the strained three-membered ring cleaves and one of the oxy-

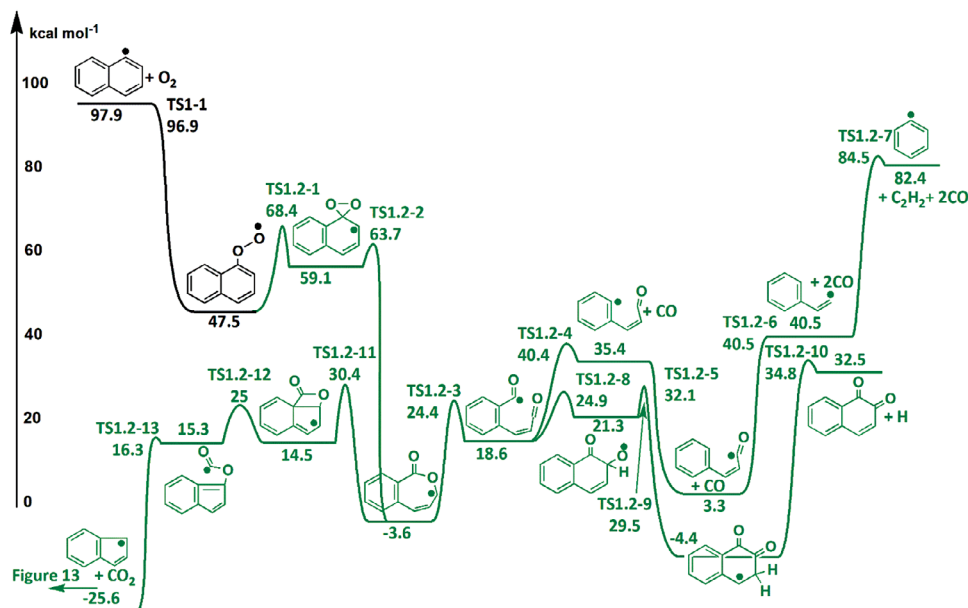


FIGURE 6 Channel 1.2: Formation and further reactions of A2•YCO2 (APFD/6-311G(d,p) calculations).

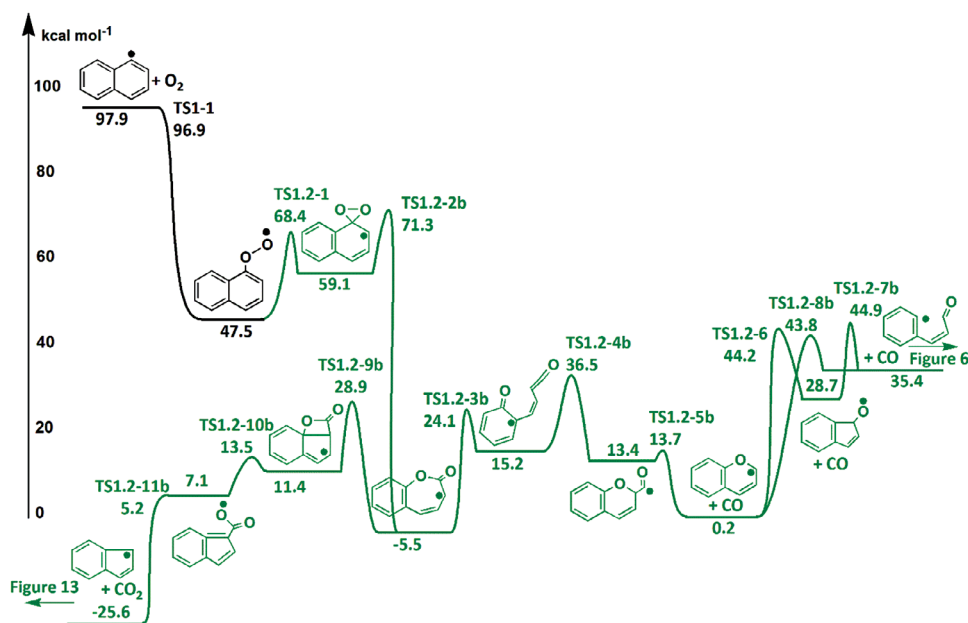


FIGURE 7 Channel 1.2 con't: Formation and further reactions of A2•YCO2. (APFD/6-311G(d,p) calculations).

gen atoms links to the closest carbon, while the other oxygen forms a C = O double bond. A little barrier of 4.7 kcal mol<sup>-1</sup> versus 13.2 kcal mol<sup>-1</sup> from<sup>18</sup> relative to A2•YCO2 (TS1.2-2) is necessary for the formation of the relatively stable AIYCDOOC•CC. These reactions correspond with those reported in Ref. 18 The energy difference between A2•YCO2 and AIYCDOOC•CC (-3.6 kcal mol<sup>-1</sup>) amounts to approximately 62 kcal mol<sup>-1</sup>, in agreement with 60.4 kcal mol<sup>-1</sup> from.<sup>18</sup>

This last adduct (AIYCDOOC•CC) undergoes the ring-opening of its seven-membered ring via TS1.2-3 through

27.3 kcal mol<sup>-1</sup> versus 33.3 kcal mol<sup>-1</sup> reported in Ref. 18 and resulting in 1,2-naphthoquinone + H. However, the calculated energy barrier for the back reaction, closure of the seven-membered ring, at 6.5 kcal mol<sup>-1</sup> is in good agreement with the G3 value of 6 kcal mol<sup>-1</sup> from Ref. 18 The energy released by the exothermic reaction allows a series of subsequent elimination reactions. A first CO elimination TS1.2-4 (22.4 kcal mol<sup>-1</sup> relative to A1C3OC•DO) is taking place resulting in A1•C3DO which undergoes an exothermic and barrier-less intramolecular H-abstraction (TS1.2-5) to a more stable isomer A1C2C•DO. Some 32 kcal

$\text{mol}^{-1}$  are released to the system and favor a second CO elimination requiring via **TS1.2-6** 37 kcal  $\text{mol}^{-1}$  to  $\text{A1C3OC}\cdot\text{DO}$  + CO. The latter radical eliminates  $\text{C}_2\text{H}_2$  (**TS1.2-7**) leading to a phenyl radical. As reported and described in Zhou et al.,<sup>18</sup> an alternative path for  $\text{A1C3OC}\cdot\text{DO}$  is a new C–C bond formation via **TS1.2-8** forming  $\text{A1ODA1O}\cdot$  at 21.3 kcal  $\text{mol}^{-1}$ . This last intermediate undergoes a H-shift through 10.8 kcal  $\text{mol}^{-1}$  (**TS1.2-9**) to a lower energy intermediate  $\text{A2}\cdot\text{DODO}$  lying at  $-4.4$  kcal  $\text{mol}^{-1}$  followed by a H-elimination (**TS1.2-10**) to the final product 1,2-naphthoquinone ( $\text{A2DODO}$ ). Overall the values calculated in this work are in very good agreement with Ref. 18 except the  $\text{A1C3OC}\cdot\text{DO}$  calculated at 18.6 kcal  $\text{mol}^{-1}$  which is lower by 5 kcal  $\text{mol}^{-1}$  than in Ref. 18. However, the value determined using the group additivity of the RMG program<sup>41</sup> results in similar low energy of 16.5 kcal  $\text{mol}^{-1}$ .

$\text{A1YCDOOC}\cdot\text{CC}$  can undergo an internal C–C bond formation (via **TS1.2-11**) inside the seven-membered ring, resulting in a five-membered ring and a four-membered ring through a 34.0 kcal  $\text{mol}^{-1}$  energy barrier relative to  $\text{A1YCDOOC}\cdot\text{CC}$  which is in excellent agreement with Ref. 18. The tricyclic radical  $\text{A1YC5}\cdot\text{YC3ODO}$  lying at 14.5 kcal  $\text{mol}^{-1}$  breaks the  $\text{YC3ODO}$  ring through ca. 11 kcal  $\text{mol}^{-1}$  (via **TS1.2-12**) leading to the intermediate  $\text{A1YC5YOC}\cdot\text{DO}$  which breaks easily the C–O bond (via **TS1.2-13**) to form  $\text{CO}_2$  and indenyl radical.

Alternatively, one of the oxygen atoms of  $\text{A2}\cdot\text{YCO}_2$  links to the carbon common to the second ring (**TS1.2-2b**) with a C–O double bond formation (Figure 7). A barrier of 12 kcal  $\text{mol}^{-1}$  relative to  $\text{A2}\cdot\text{YCO}_2$  (**TS1.2-2b**) is required for the formation of  $\text{A1YCDOOC}\cdot\text{CCb}$ . As reported in Ref. 18 two paths are available to this relatively stable intermediate. The first one is through the ring opening of  $\text{A1YCDOOC}\cdot\text{CCb}$  via (**TS1.2-3b**) followed by the attack of the radical on the C–O bond to the formation of a bicycle  $\text{A1YC5}\cdot\text{OCDO}$  (**TS1.2-4b**). This last intermediate loses CO almost without barrier (**TS1.2-5b**) to  $\text{A1YC5}\cdot\text{O}$ . A detailed discussion is reported by Zhou et al. in Ref. 18. In this work further dissociation reactions of  $\text{A1YC5}\cdot\text{O}$  have been investigated:  $\text{A1YC5}\cdot\text{O}$  can undergo an internal C–C bond formation (**TS1.2-6b**), losing CO simultaneously and forming a five-membered ring which opens resulting in the  $\text{A1C3OC}\cdot\text{DO}$  radical over some 44 kcal  $\text{mol}^{-1}$  (**TS1.2-7b**).  $\text{A1YC5}\cdot\text{O}$  can also directly open to  $\text{A1C3OC}\cdot\text{DO}$  (**TS1.2-8b**). Further reactions of  $\text{A1C3OC}\cdot\text{DO}$  are described in Figure 6.

Similarly to the path described in Figure 6,  $\text{A1YCDOOC}\cdot\text{CCb}$  can undergo the same internal C–C bond formation (via **TS1.2-9b**) inside the seven-membered ring, to  $\text{A1YC5}\cdot\text{YC3ODOb}$  through 34.4 kcal  $\text{mol}^{-1}$  energy barrier relative to  $\text{A1YCDOOC}\cdot\text{CCb}$ , here again in excellent agreement with Ref. 18. The tricyclic radical  $\text{A1YC5}\cdot\text{YC3ODOb}$  breaks the C–O bond of the  $\text{YC3ODO}$

ring through only 2.1 kcal  $\text{mol}^{-1}$  (**TS1.2-10b**) leading to  $\text{A1YC5CO}_2\cdot$  which dissociates easily (**TS1.2-11b**) to form  $\text{CO}_2$  and the indenyl radical.

### 3.2.4 | Formation of $\text{A2}\cdot\text{YC3O}_2$ through addition of oxygen atom to adjacent ring (Channel 1.3)

Figure 8 illustrates the intermediate species resulting from the attack of the terminal oxygen in the peroxy group at the nearest carbon atom situated on the adjacent ring. From this addition, a relatively stable five-membered ring intermediate,  $\text{A2}\cdot\text{YC3O}_2$ , is formed with an enthalpy of formation of 65.2 kcal  $\text{mol}^{-1}$  via an energy barrier of 32 kcal  $\text{mol}^{-1}$  (**TS1.3-1**) relative to  $\text{A2OO}\cdot$ .

This intermediate reacts in a number of subsequent steps, starting by breaking the weak and strained O–O bond via **TS1.3-2** (only 8.6 kcal  $\text{mol}^{-1}$  relative to  $\text{A2}\cdot\text{YC3O}_2$ ) and forming a lower energy bicyclic radical,  $\text{A1}\cdot\text{DOA1YC2O}$  (20.2 kcal  $\text{mol}^{-1}$ ). We note that, unlike in the previously discussed channels, the two oxygen atoms are no longer on the same ring after the addition reaction. This new formed intermediate can open the bicycle over a 23.2 kcal  $\text{mol}^{-1}$  barrier (**TS1.3-3**) followed by an opening of one ring (**TS1.3-4**) to  $\text{A1DODC}\cdot\text{C3DO}$  at an energy level of 63.6 kcal  $\text{mol}^{-1}$ . A further reaction sequence involves an exothermic hydrogen-shift from the vinyl group to the carboxylic group to a lower energetic isomer  $\text{RC3}\cdot\text{DO}$  at an energy level of 21.6 kcal  $\text{mol}^{-1}$ . Further reaction steps of  $\text{RC3}\cdot\text{DO}$  involve elimination of CO and  $\text{C}_2\text{H}_2$  via **TS1.3-5** and **TS1.3-6**, respectively. Alternatively to **TS1.3-4**, a hydrogen elimination can take place via **TS1.3-8** to a stable product o- $\text{A1DOA1DO}$ .

Unlike in the previously discussed reaction channels instead of the phenyl radical, a methylene-cyclohexadienyl-ketone radical ( $\text{A1}\cdot\text{DODC}$ ) is formed. Further reactions of this intermediate are not investigated in this study. We note that channel 1.3 is not forming a phenyl radical.

### 3.2.5 | Formation of $\text{A2}\cdot\text{OOH}$ through intramolecular H-abstraction by the oxygen atom (Channel 1.4)

The formation of a reactive ortho-hydroperoxy-naphthyl radical  $\text{A2}\cdot\text{OOH}$  occurs via **TS1.4a-1** through the intramolecular abstraction of the hydrogen from the same ring as the peroxy group. The formation of  $\text{A2}\cdot\text{OOH}$  occurs through a loose cyclic five-membered ring structure (Figure 9). This abstraction has a barrier which is 14.3 kcal  $\text{mol}^{-1}$  below the entrance channel and is accessible to



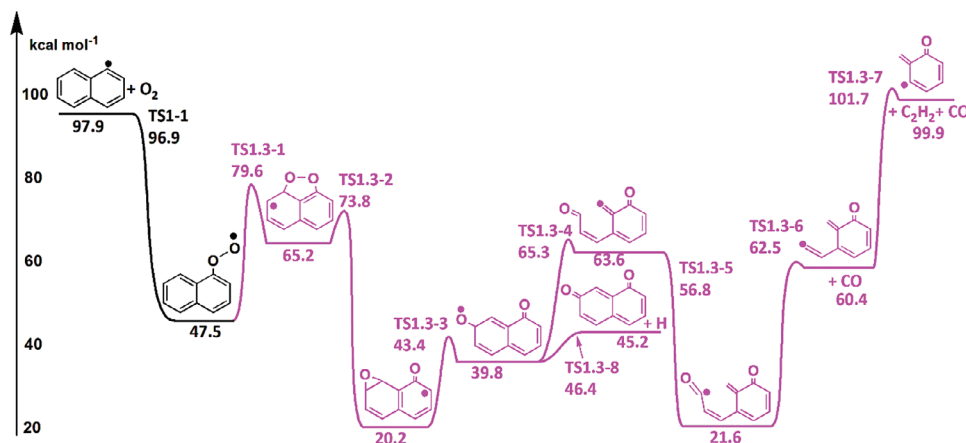


FIGURE 8 Channel 1.3: Formation and further reactions of A2•YC3O2 (APFD/6-311G(d,p) calculations).

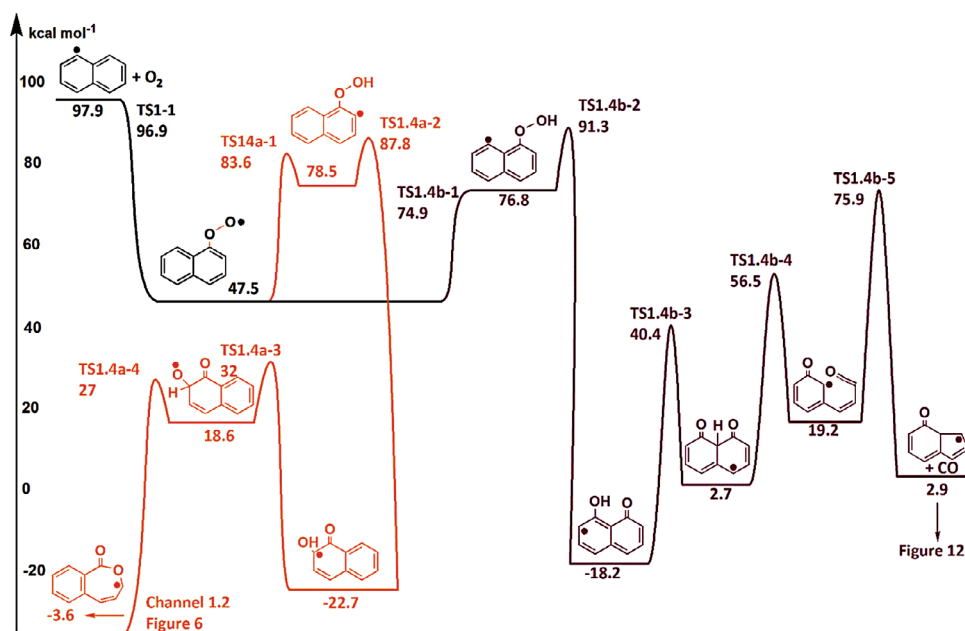


FIGURE 9 Channel 1.4: Formation and further reactions of A2•OOH (APFD/6-311G(d,p) calculations).

the chemically activated naphthyl-peroxy radical A2OO•. In a subsequent step the OH-group is transferred from A2•OOH-a to the radical site on the carbon atom of the same ring via **TS1.4a-2** (9.3 kcal mol<sup>-1</sup>). This step is connected with a release of energy to the system of approximately 70 kcal mol<sup>-1</sup> and the formation of a cyclic hydroxyl-ketone radical, A1A1•OHDO, at an energy level of -22.7 kcal mol<sup>-1</sup>. The available excess of energy enables a second hydrogen transfer reaction via **TS1.4a-3** (55 kcal mol<sup>-1</sup>) resulting in A1A1O•DO. The latter undergoes further reaction via **TS1.4a-4** forming the same intermediate species A1YCDOOC•CC as appearing in channel 1.2, see Section 3.2.3.

A second reaction sequence involves the abstraction of a hydrogen from A2OO• from the adjacent ring (**TS1.4b-1**). The hydrogen moves from the neighboring ring to the

oxygen radical of A2OO• through a six-membered ring structure. This forms the hydroperoxide radical A2•OOH-b at approximately the same energy level of 76.8 kcal mol<sup>-1</sup> as the A2•OOH-a isomer. Surprisingly, no saddle point has been calculated for this abstraction reaction. The calculations show also that the energy of **TS1.4b-1** is lower than that of **TS1.4a-1**. This difference can be easily explained by the structure of both transition states: **TS1.4b-1** involves a six-membered ring structure while **TS1.4a-1** a more strained five-membered ring. The difference in the structure of the transition states, however, cannot explain the barrier-less hydrogen abstraction via **TS1.4b-1**.

Calculations for subsequent reaction steps of the A2•OOH-b isomer (Figure 9) indicate a transition state structure **TS1.4b-2** for the intramolecular transfer of the hydroxyl group OH to the radical site on the adjacent ring

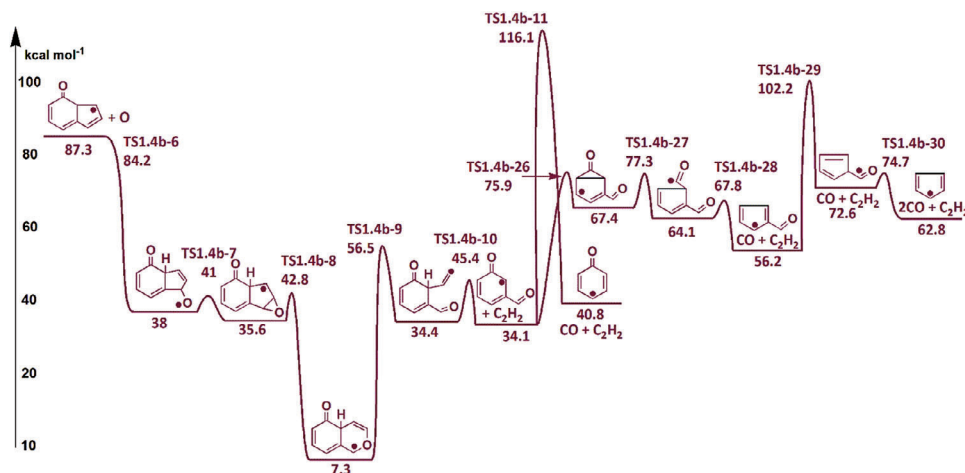


FIGURE 10 Channel 1.4b (continued): Formation and further reactions of A1DOYC5O• (APFD/6-31IG(d,p) calculations).

(14.5 kcal mol<sup>-1</sup>), resulting in a low energetic A1•OHA1DO at an energy level of -18.2 kcal mol<sup>-1</sup>. This species rearranges by moving the hydrogen of OH via **TS1.4b-3** to allow the formation of a C O double bond and resulting in A1DOA1•DO at an energy level of 2.7 kcal mol<sup>-1</sup>. Further reactions of A1DOA1•DO consist of a ring opening and a CO elimination through **TS1.4b-4** (54 kcal mol<sup>-1</sup>) and **TS1.4b-5** (57 kcal mol<sup>-1</sup>), respectively resulting in the radical species A1DOYC5•.

A possible subsequent reaction of A1DOYC5• is the addition of an oxygen atom to the cyclopentadienyl ring of the A1DOYC5• forming A1DOYC5O•, as illustrated in Figure 10 and Table A. As previously established, the oxygen addition proceeds without barrier with an excess of energy of 50 kcal mol<sup>-1</sup> (**TS1.4b-6**).

This oxygen radical of the A1DOYC5O• intermediate attacks the adjacent carbon by breaking the double bond and forming a bicycle A1DOYC5•YC2O over a barrier of only 3 kcal mol<sup>-1</sup> (**TS1.4b-7**) immediately followed by the opening of the bicycle over 7.4 kcal mol<sup>-1</sup> (**TS1.4b-8**). The formation of the radical intermediate A1DOYC2OC• at an energy level of 7.3 kcal mol<sup>-1</sup> releases 28 kcal mol<sup>-1</sup>, which is sufficient to open the first ring via **TS1.4b-9** requiring 50 kcal mol<sup>-1</sup>. The elimination of CO and C<sub>2</sub>H<sub>2</sub> then takes place via **TS1.4b-10** and **TS1.4b-11** to 2-5ODYC6•, which is a resonance stabilized phenoxy radical. As can be seen in Figure 10, the CO elimination taking place via **TS1.4b-11** proceeds via a high energy barrier. In parallel, another path at lower energy is possible through the formation of a fused-tricyclic radical over ca. 42 kcal mol<sup>-1</sup> (**TS1.4b-26**). The strained tricyclic radical (YC5•COYC3DO) undergoes the easy opening of the three-membered ring (**TS1.4b-27**) to form YC5COC•DO lying at 64.1 kcal mol<sup>-1</sup>. This last radical eliminates CO over only 4 kcal<sup>-1</sup> (**TS1.4b-28**). After an intramolecular H-shift (**TS1.4b-29**) via a 46 kcal mol<sup>-1</sup>

energy barrier, a second CO elimination is taking place (**TS1.4b-30**) resulting in a cyclopentadienyl YC5• + CO.

The further addition of an oxygen atom to 2-5-ODYC6• radical takes place as expected without barrier and releases 66 kcal mol<sup>-1</sup> of energy (see Figure 11). Subsequent reactions of this phenoxy radical, 2-5-ODYC6O•, follow the same scheme as the previous ones: forming a bicycle over a barrier of 12 kcal mol<sup>-1</sup> (**TS1.4b-13**), followed by the formation of a 7-membered ring radical 25ODYC6•O at an energy level of -1.2 kcal mol<sup>-1</sup> via **TS1.4b-14**. Opening the 7-membered ring requires a comparatively high energy of 43 kcal mol<sup>-1</sup> (**TS1.4b-15**) relative to 25ODYC6O• and results in ODC4DOC2• at an energy level of 26.9 kcal mol<sup>-1</sup>. This species undergoes a series of elimination reactions starting with C<sub>2</sub>H<sub>2</sub> elimination (**TS1.4b-16**), CO elimination (**TS1.4b-17**) and C-C bond scission (**TS1.4b-18**) to the final products C<sub>2</sub>H<sub>2</sub> + CH O.

The other plausible path for the 2-5-ODYC6O• radical is the intramolecular H-shift over only 6.3 kcal mol<sup>-1</sup> (**TS1.4b-19**) to form ODA1•DO at -14.3 kcal mol<sup>-1</sup>. A favorable subsequent reaction is the formation of a three-membered ring ODYC5•YC3DO over 25 kcal mol<sup>-1</sup> (**TS1.4b-20**). The radical ODYC5•YC3DO lying at 3.5 kcal mol<sup>-1</sup> opens the strained three-membered ring (**TS1.4b-21**) via 4 kcal mol<sup>-1</sup>, to form a more stable ODYC5C•DO at -11.8 kcal mol<sup>-1</sup>. The subsequent reactions are CO elimination (**TS1.4b-22**), opening of the five-membered ring (**TS1.4b-23**) via some 30 kcal mol<sup>-1</sup> and a series of eliminations to the final products C<sub>2</sub>H<sub>2</sub>, 2CO and CH<sub>2</sub> = CH•.

Since oxygen is available in the system, abstraction reactions of one hydrogen by O<sub>2</sub> or O are also taking place leading to para-quinone + HO<sub>2</sub> and para-quinone + OH, respectively (this last reaction is not represented in the diagram but is included in Table 1).

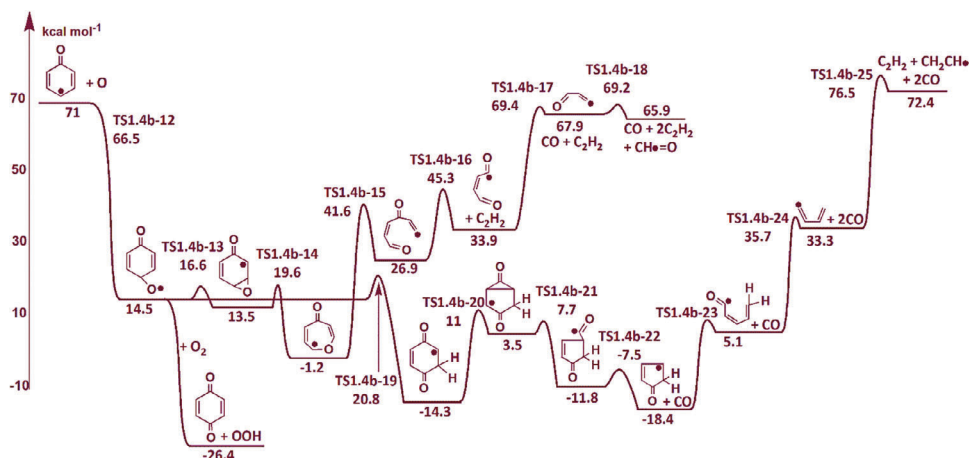


FIGURE 11 Channel 1.4b (continued): Formation and further reactions of 2-5-ODYC6O• (APFD/6-311G(d,p) calculations).

### 3.2.6 | Formation of A2•DO through RO–O bond cleavage (Channel 2)

The dissociation of the peroxy A2OO• radical to A2O• + O is calculated to be 31.3 kcal mol<sup>-1</sup> endothermic relative to the stabilized A2OO• radical but still 19 kcal mol<sup>-1</sup> below the initial state A2• + O<sub>2</sub>. O–O bond dissociation reported in Ref. 18 is at 29.1 kcal mol<sup>-1</sup> at B3LYP/6-311G\*\* level and 28.9 kcal mol<sup>-1</sup> at G3 level which is ca. 2 kcal mol<sup>-1</sup> lower than our calculations. The calculations indicate no saddle point (TS2-1) for this reaction. This result is similar to that obtained for phenyl and other radicals in previous studies.<sup>4,5,42,43</sup> The O–O bond cleavage has a loose transition state and is important in combustion. Due to the possible resonance between the oxygen radical and the phenyl ring, a C–O double bond is formed and the radical site moves to the ring. The radical A2O• rearranges to a more stable A2•DO. The energy value of the A2•DO radical (24.3 kcal mol<sup>-1</sup>) is in excellent agreement with the G3-value from Zhou et al.<sup>18</sup> Subsequent reactions of the naphthoxy radical (A2O•) or A2•DO are examined and discussed in Section 3.3.

## 3.3 | Reactions of 1-naphthyl radical A2• (C<sub>10</sub>H<sub>7</sub>•) with O

Figure 3 illustrates the main reaction channels resulting from the addition of an oxygen atom to A2• (A2• + O). The primary adduct A2O• rearranges to a more stable A2•DO. All subsequent reactions listed in Figure 3 conduct mainly to a phenyl radical, CO and acetylene. The addition of the oxygen atom to A2• and the primary pathways resulting from the further reactions of the peroxy radical A2OO•, see Figure 3, include:

**Channel 3:** Addition of an oxygen atom to A2• forming A2O• and A2•DO (TS3-1)

**Channel 3.1:** Further reactions of A2•DO (TS3.1-1)

**Channel 3.2:** Further reactions of A2•DO (TS3.2-1)

**Channel 3.3:** Further reactions of A2•DO (TS3.3-1)

**Channel 3.4:** Addition of an oxygen atom to A2•DO forming A2O•DO (TS3.4-1)

The different reaction paths are described in detail in the following sections.

### 3.3.1 | Addition of an oxygen atom to A2• forming A2O• and A2•DO (Channel 3)

In Table A the formation of A2•DO is illustrated through the dissociation of A2O–O• to A2O• (which rearranges to A2•DO) + O (TS2-1). Assuming that some oxygen atoms are available in the system, the second plausible formation pathway of A2•DO constitutes the addition of an oxygen atom directly to the naphthyl radical A2• (TS3-1) as illustrated in Table A. The calculated barrier for the oxygen addition via TS3-1 reveals ca. 12 kcal mol<sup>-1</sup> relative to the A2• + O entrance channel, while 32 kcal mol<sup>-1</sup> are required for O–O dissociation (TS2-1). However, for these two competitive pathways, the energy level of the entrance channel A2• + O is at 158 kcal mol<sup>-1</sup> versus A2OO• at 47.5 kcal mol<sup>-1</sup>, which may determine strongly the occurrence of the channel. In this study both reactions are considered.

### 3.3.2 | Further reactions of A2•DO (Channel 3.1)

The intermediate species A2•DO undergoes a transformation via a bicyclic structure (A2•YC2O) over a relatively high energy barrier of 63.1 kcal mol<sup>-1</sup> (TS3.1-1) relative to A2•DO, see Figure 12. Breaking the strong C–O double bond explains the magnitude of this barrier. The channel leading

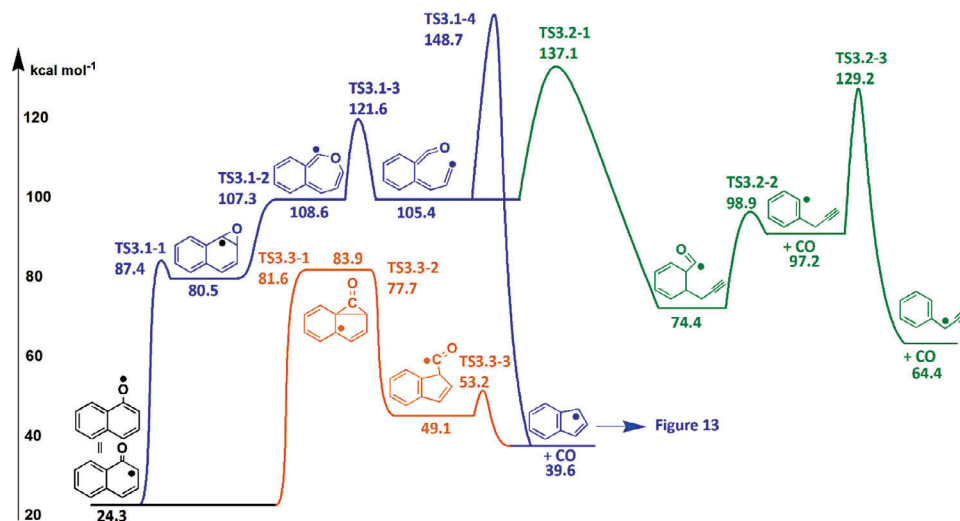


FIGURE 12 Channel 3.1, Channel 3.2, and Channel 3.3: Formation and further reactions of A2•DO (APFD/6-311G(d,p) calculations).

to the formation of an indenyl radical is different from that identified and reported in Ref. 18 Zhou et al. have identified the direct formation of a fused tricyclic compound containing a cyclopentene ring through a similar barrier 61.1 kcal mol<sup>-1</sup> (at B3LYP/6-311G\*\* level). This last intermediate lies at 61.7 and 57.7 kcal mol<sup>-1</sup> at B3LYP/6-311G\*\* and G3 levels respectively above A2•DO which is slightly higher than the identified A2•YC2O in this work at 56.2 kcal mol<sup>-1</sup>. Investigation of the formation of the fused tricyclic compound is reported in Section 3.3.4.

Once formed, A2•YC2O opens the bicycle and forms without saddle point (TS3.1-2) a seven-membered ring A1YC•OC3 at an energy level of 108.6 kcal mol<sup>-1</sup>. The latter species opens the seven-membered ring via TS3.1-3 to form A1DCDOC3• at approximately the same level of energy. Subsequent reactions of A1DCDOC3• involve two paths. The first path is a CO elimination over ca. 43 kcal mol<sup>-1</sup> barrier (TS3.1-4) forming an indenyl radical A1YC5•.

The cyclopentadienyl ring of the indenyl radical A1YC5• can be attacked by a further oxygen atom forming A1YC5O•, see Figure 13. This addition proceeds without barrier and releases an excess of energy of near 66 kcal mol<sup>-1</sup> (TS3.1-5). The intermediate A1YC5O• rearranges through its resonance structure to an energetically lower isomer A1•YC5DO via a low barrier of 5.2 kcal mol<sup>-1</sup> (TS3.1-6). A1•YC5DO with the radical site inside the phenyl ring undergoes ring-opening of the five-membered ring over a low energy barrier of ca. 9 kcal mol<sup>-1</sup> (TS3.1-7) to the isomer A1C2C•DO, see Figure 13. The subsequent reactions of this species leading to phenyl, CO and C2H2 occur also in Channel 1.2 and are described in Section 3.2.3 and Figure 6.

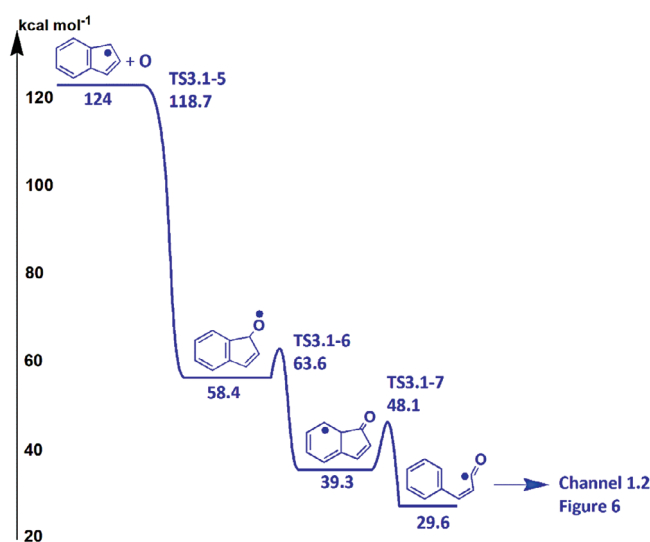


FIGURE 13 Channel 3.1 (continued): Oxidation of A1YC5• to formation and further reactions of A1YC5O• (APFD/6-311G(d,p) calculations).

### 3.3.3 | Further reactions of A2•DO (Channel 3.2)

The reaction Channel 3.2 is identical with Channel 3.1 up to the species A1DCDOC3•. The second path available to the A1DCDOC3• radical is through an internal rotation of the vinyl group followed by an H-shift over an energy barrier of some 32 kcal mol<sup>-1</sup> (TS3.2-1), see Figure 12 and the subsequent formation of a triple C≡C bond. This is followed by the elimination of CO over TS3.2-2 to form A1•C2TC. Here again, the radical with a resonance structure transfers the H-atom (see Figure 12) from the

propargyl-group ( $\text{CH}_2\text{C}\equiv\text{CH}$ ) to the phenyl ring. This step requiring an energy of some  $36 \text{ kcal mol}^{-1}$  (TS3.2-3) forms the A1C•CTC isomer at lower energy.

### 3.3.4 | Further reactions of A2•DO (Channel 3.3)

A plausible subsequent reaction of the naphthoxy radical A2•DO (similarly to Ref. 18) is the formation of a fused tricyclic radical A1•YC5YC3DO via a  $57.3 \text{ kcal mol}^{-1}$  energy barrier (TS3.3-1) which is in very good agreement with the  $57.8 \text{ kcal mol}^{-1}$  value (G3 calculations) reported by Zhou et al.,<sup>18</sup> see Figure 12. The radical A1YC5•YC3DO is lying  $59.6 \text{ kcal mol}^{-1}$  above A2•DO, which is higher by  $1.9 \text{ kcal mol}^{-1}$  than the value reported by Zhou et al. This last radical opens the strained three-membered ring (TS3.3-2) barrierless, while Ref. 18 reports a  $0.5 \text{ kcal mol}^{-1}$  energy barrier to form a more stable A1YC5C•DO at  $24.8 \text{ kcal mol}^{-1}$  relative to A2•DO.

The subsequent reaction constitutes CO elimination (TS3.3-3) via a  $28.9 \text{ kcal mol}^{-1}$  energy barrier above A2•DO versus  $31.9 \text{ kcal mol}^{-1}$  at G3 level from Zhou et al. The resulting products, indenyl radical A1YC5• + CO, are formed at  $15.7 \text{ kcal mol}^{-1}$  ( $14.5 \text{ kcal mol}^{-1}$  in Ref. 18) above the naphthoxy radical A2•DO.

### 3.3.5 | Addition of an oxygen atom to A2•DO forming para-A2O•DO (Channel 3.4)

In Sections 3.3.2–3.3.4 (Channel 3.1–3.3), the transformation and decomposition reactions of the naphthalenoxy-radical ortho-A2•DO have been reported. To explore all plausible reactions during the oxidation of A2•, the addition of an oxygen atom to the A2•DO radical (TS3.4-1) has been examined (Channel 3.4, see Figure 14 and Table A for illustration). The oxygen can be added to a carbon atom in ortho- or para- position relative to the C-O site, see Figure 14. The meta-position is not favored because of missing resonance inside the ring and, therefore, has not been considered in this study. The ortho-addition of the oxygen atom gives the same intermediate species as appearing in Channel 1.1 (Figure 5) and Channel 1.2 (Figure 6). The subsequent reactions of these species have been discussed in Sections 3.2.2 and 3.2.3. The para-addition of the O-atom to A2•DO releases  $61 \text{ kcal mol}^{-1}$  excess energy, which favors subsequent reactions. The radical para-A2O•DO lying at  $18.3 \text{ kcal mol}^{-1}$ , undergoes an easy electron rearrangement and forms a bicycle over TS3.4-2 (ca.  $5 \text{ kcal mol}^{-1}$ ) to A2DOC•YC2O at an energy level of  $15.2 \text{ kcal mol}^{-1}$ . This reaction step is followed by ring opening reactions and finally

$\text{C}_2\text{H}_2$  and CO eliminations and formation of the phenyl radical.

As shown previously in Figures 10–12, para-A2O•DO may undergo an intramolecular H-shift (TS3.4-9) to form ODA1•DOA1, lower in energy than A2O•DO at  $-9.6 \text{ kcal mol}^{-1}$ . Similar to the channels described in Figures 10–12, the formation of a fused-tricyclic compound is taking place over ca.  $35 \text{ kcal mol}^{-1}$  (TS3.4-10) followed by the barrierless opening of the three-membered ring (TS3.4-11) to form A1ODYC5•DO at  $-6.2 \text{ kcal mol}^{-1}$ . The subsequent reactions are CO elimination (TS3.4-12) followed by the opening of the five-membered ring via a relatively high barrier of  $63 \text{ kcal mol}^{-1}$  (TS3.4-13). Two CO and  $\text{C}_2\text{H}_2$  elimination reactions lead to the final products  $\text{C}_6\text{H}_5\bullet + 2\text{CO} + \text{C}_2\text{H}_2$ .

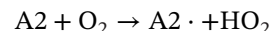
## 4 | REACTION RATE COEFFICIENTS

The reaction rate coefficients reported in this study were estimated using the canonical transition state theory (TST) and are listed in Table 1. The ThermKin code<sup>34</sup> is used to calculate the rate coefficients of the elementary reactions given in the modified Arrhenius form, see Table 1, for the temperature range from 300 to 2000 K

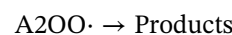
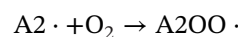
$$k = A \cdot T^b \cdot \exp(-E_A/T).$$

From the kinetic analysis, high-pressure rate constants for each reaction are obtained from the calculated energies, vibration frequencies, and structures. The modified Arrhenius parameters are determined from least squares regression analysis. Entropy differences between the reactants and transition states are used to determine the pre-exponential factors A via canonical TST.

Table 1 lists the calculated kinetic parameters for the activation reactions of A2 involving  $\text{O}_2$  and O, OH, H,  $\text{HO}_2$



High-pressure-limit kinetic parameters for the forward reactions of A2• for the reactions involving  $\text{O}_2$



as well as involving O

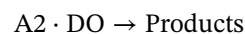
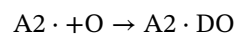


TABLE 1 Calculated reaction rate coefficients<sup>a</sup> for the reactions discussed in Section 3. For CHEMKIN use a radical is identified with “J.”

No	Reactions	A	b	E <sub>A</sub>
<b>Reactions starting with A2</b>				
	A2 + O2 = A2J + HO2	7.1468E+01	2.98	69.60
	A2 + HO2 = A2J + H2O2	1.0344E+01	3.48	17.45
	A2 + OH = A2J + H2O	5.3763E+02	2.91	-7.34
	A2 + O = A2J + OH	4.7817E+08	1.04	22.33
	A2 + H = A2J + H2	3.1864E+10	.80	12.87
<b>Reactions starting with A2J</b>				
<b>Channel-1</b>				
1	A2J + O2 = A2OOJ	4.1336E+00	2.99	-1.568
<b>Channel 1.1</b>				
2	A2OOJ = A2JYC2O2	6.3318E+11	0.320	44.27
3	A2JYC2O2 = A2OJCDO	4.0633E+12	0.176	-3.68
4	A2OJCDO = A2DOYC2OCJ	9.7646E+12	-0.09	3.96
5	A2DOYC2OCJ = A1YC2OCJCDO	2.0841E+12	0.30	13.39
6	A1YC2OCJCDO = A1CCJCDOCDO	1.2189E+12	0.77	28.61
7	A1CCJCDOCDO = A1JCDOCDO + C2H2	8.9536E+11	0.75	46.37
8	A1JCDOCDO = A1CDOCJDO	3.8021E+11	0.54	4.39
9	A1CDOCJDO = A1CJDO + CO	2.2066E+13	0.31	8.58
10	A1CJDO = A1J + CO	1.2154E+14	0.507	25.06
11	A1CCJCOCO = A1YC5OJCO	1.9450E+12	-0.1	11.42
12	A1YC5OJCO = A1YC5DO + HCO	1.8998E+12	0.3	0.53
13	A2OJCDO = A1YCDOOCJCC Further reactions in Channel 1.2	2.9910E+12	0.04	9.05
<b>Channel 1.2</b>				
14	A2OOJ = A2JYCO2	8.4937E+11	0.35	21.41
15	A2JYCO2 = A1YCDOOCJCC	4.5442E+12	0.14	5.199
16	A1YCDOOCJCC = A1C3OCJDO	1.4034E+11	0.24	27.86
17	A1C3OCJDO = A1JC3DO + CO	1.4575E+13	0.41	22.98
18	A1JC3DO = A1C2CJDO	3.1351E+10	0.56	-3.02
19	A1C2CJDO = A1CDCJ + CO	4.7566E+13	0.46	37.76
20	A1CDCJ = A1J + C2H2	3.3201E+13	0.74	44.41
Reactions based on Ref. 18				
Reaction resulting from Figure 6				
21	A1YCDOOCJCC = A1YC5JYC3ODO	2.0250E+13	1.30	34.47
22	A1YC5JYC3ODO = A1YC5OCJDO	2.5000E+15	1.09	11.08
23	A1YC5OCJDO = A1YC5J + CO2	9.1934E+14	1.32	1.55
24	A1C3OCJDO = A1ODA1OJ	1.0397E+09	3.69	6.78
25	A1ODA1OJ = A2JDODO	1.5588E+14	1.35	8.65
26	A2JDODO = A2DODO + H	7.5203E+10	3.09	38.82
Reactions resulting from Figure 7				
27	A2JYCO2 = A1YCDOOCJCCB	5.4468E+14	1.34	12.85
28	A1YCDOOCJCCB = A1YC5JYC3ODOB	2.9466E+13	1.32	34.78
29	A1YC5JYC3ODOB = A1YC5CO2J	2.7325E+15	1.04	2.64
30	A1YC5CO2J = A1YC5J + CO2	1.7897E+14	1.20	-1.65
31	A1YCDOOCJCCB = A1YC5JOCDO	3.4238E+14	1.43	42.46

(Continues)

TABLE 1 (Continued)

No	Reactions	A	b	E <sub>A</sub>
32	A1YC5JOCDO = A1YC5JO + CO	1.4520E+15	1.27	0.73
33	A1YC5JO = A1JC3DO	2.6467E+16	1.28	41.84
34	A1YC5JO = A1YC5OJ	2.0894E+14	1.35	44.50
35	A1YC5OJ = A1JC3DO	2.1930E+15	1.26	16.79
<b>Channel 1.3</b>				
36	A2OOJ = A2JYC3O2	1.4626E+11	0.42	32.57
37	A2JYC3O2 = A1JDOA1YC2O	1.9762E+12	0.402	9.06
38	A1JDOA1YC2O = A1DOA1OJ	8.1461E+12	0.184	23.77
39	A1DOA1OJ = A1DODCJC3DO	3.9404E+12	0.51	26.00
40	A1DODCJC3DO = RC3JDO	2.2917E+13	-0.69	-5.88
41	RC3JDO = A1DODCC2J + CO	3.9115E+13	0.503	41.43
42	A1DODCC2J = A1JDODC + C2H2	9.7567E+12	0.736	42.18
43	A1DOA1OJ = O*A1OA1O	1.3855E+11	1.086	5.53
<b>Channel 1.4</b>				
<b>Channel 1.4a</b>				
44	A2OOJ = A2JOOH-a	8.2030E+10	0.719	36.35
45	A2JOOH-a = A1A1JOHDO	4.5277E+08	1.505	10.94
46	A1A1JOHDO = A1A1OJDO	9.1078E+11	0.468	54.35
47	A1A1OJDO = A1YCDOOCJCC	2.9910E+12	0.045	9.03
<b>Channel 1.4b</b>				
48	A2OOJ = A2JOOH-b	1.6254E+10	0.876	27.56
49	A2JOOH-b = A1JOHA1DO	1.1519E+09	1.346	16.38
50	A1JOHA1DO = A1DOA1JDO	3.8098E+11	0.468	58.87
51	A1DOA1JDO = A1JDOC4DO	1.1541E+13	0.430	54.29
52	A1JDOC4DO = A1DOYC5J + CO	7.7931E+11	0.879	56.99
Addition of an oxygen atom to A1DOYC5J				
53	A1DOYC5J + O = A1DOYC5OJ	1.5676E+07	1.391	-4.72
54	A1DOYC5OJ = A1DOYC5JYC2O	1.7444E+12	0.154	3.36
55	A1DOYC5JYC2O = A1DOYC2OCJ	2.3528E+12	0.244	7.90
56	A1DOYC2OCJ = A1DOC2JCDO	1.3096E+14	-0.344	55.12
57	A1DOC2JCDO = A1JDOCDO + C2H2	8.4027E+11	0.573	11.47
58	A1JDOCDO = 25ODYC6J + CO	2.0722E+12	0.782	82.40
59	A1JDOCDO = YC5JCOYC3	1.0070E+12	.45	42.27
60	YC5JCOYC3 = YC5COCJDO	1.2421E+13	.088	10.53
61	YC5COCJDO = YC5JCDO + CO	2.7014E+12	.352	42.60
62	YC5JCDO = YC5CJDO	7.1032E+11	.375	46.38
63	YC5CJDO = YC5J + CO	1.4157E+12	.331	2.59
Addition of an oxygen atom to 25ODYC6J				
64	25ODYC6J + O = 25ODYC6OJ	1.0128E+07	1.482	-11.38
65	25ODYC6OJ = 25ODYC6JYC2O	5.4568E+12	0.028	12.74
66	25ODYC6JYC2O = 25ODYC6JO	1.4086E+12	0.336	6.62
67	25ODYC6JO = ODC4DOC2J	2.9596E+11	0.691	49.26
68	ODC4DOC2J = ODC3CJDO + C2H2	3.3708E+11	0.726	19.51
69	ODC3CJDO = ODC3J + CO	5.0254E+13	0.561	36.05
70	ODC3J = HCO + C2H2	1.0139E+12	0.867	29.41
71	ODYC6OJ25 = ODA1JDO	4.9618E+11	.421	6.73

(Continues)

TABLE 1 (Continued)

No	Reactions	A	b	$E_A$
72	ODAIJDO = OYC5JYC3O	3.0051E+11	.264	25.79
73	OYC5JYC3O = ODYC5CJDO	9.3505E+12	.059	4.85
74	ODYC5CJDO = ODYC5J + CO	1.3523E+12	.379	4.78
75	ODYC5J = CDCCDCCJO	3.0695E+12	.383	27.07
76	CDCCDCCJO = CDCCDCJ + CO	1.1819E+14	.470	39.19
77	CDCCDCJ = C2H3 + C2H2	2.8541E+12	1.013	44.09
78	ODYC6OJ25 + O = QUINONE + OH	7.9520E+02	2.767	-22.49
79	ODYC6OJ25 + O2 = QUINONE + HO2	1.7711E+02	2.755	-3.22
<b>Channel 2</b>				
80	A2OOJ = A2JDO + O	3.0873E+12	0.48	31.83
<b>Channel 3</b>				
81	A2J + O = A2JDO	3.0216E+07	1.10	10.87
<b>Channel 3.1</b>				
82	A2JDO = A2JYC2O	3.0961E+12	0.21	63.53
83	A2JYC2O = A1YCJOC3	5.4892E+11	0.59	27.20
84	A1YCJOC3 = A1DCDOC3J	1.0082E+12	0.49	13.46
85	A1DCDOC3J = A1YC5J + CO	2.0480E+13	0.69	43.78
86	A1YC5J + O = A1YC5OJ	1.0667E+07	1.40	-6.51
87	A1YC5OJ = A1JYC5DO	2.4293E+11	0.45	5.57
88	A1JYC5DO = A1C2CJDO	8.1425E+12	0.18	9.45
<b>Channel 3.2</b>				
89	A1DCDOC3J = A1CJOCCTC	1.9278E+11	0.499	32.09
90	A1CJOCCTC = A1JC2TC + CO	5.0515E+12	1.46	24.38
91	A1JC2TC = A1CJCTC	3.3502E+10	0.71	32.201
<b>Channel 3.3</b>				
92	A2JDO = A1JYC5YC3DO	5.0918E+11	0.55	56.17
93	A1JYC5YC3DO = A1YC5CJDO	8.3313E+12	0.006	-4.44
94	A1YC5CJDO = A1YC5J + CO	4.0755E+12	0.35	-0.57
<b>Channel 3.4</b>				
95	A2JDO + O = A2OJDO	1.8390E+05	1.764	-19.85
96	A2OJDO = A2DOCJYC2O	5.6870E+12	0.017	0.61
97	A2DOCJYC2O = A1YCDOC2OCJ	1.7018E+12	0.344	11.22
98	A1YCDOC2OCJ = A1CDOCDOC2J	1.7165E+11	0.88	36.69
99	A1CDOCDOC2J = ODCA1CJDO + C2H2	1.1039E+12	0.688	21.34
100	ODCA1CJDO = A1JCDO + CO	2.3868E+14	0.456	24.70
101	A1JCDO = A1CJDO	1.1652E+11	0.606	26.91
102	A1CJDO = AIJ + CO	1.2154E+14	0.507	25.06
103	A2OJDO = ODA1JDOA1	7.7508E+10	1.025	9.58
104	ODA1JDOA1 = AOYC5JC3O	1.4699E+11	.388	35.51
105	AOYC5JC3O = A1OYC5CJO	6.2531E+12	.0608	0.00
106	A1OYC5CJO = A1ODYC5J + CO	1.9310E+12	.391	6.73
107	A1ODYC5J = A1CJDOCDC	4.0971E+12	.294	30.54
108	A1CJDOCDC = AIJCDC + CO	7.1370E+14	.481	26.13
109	AIJCDC = A1CDCJ	3.6127E+10	.656	21.25
110	A1CDCJ = AIJ + C2H2	8.2314E+11	1.291	44.11
111	A2OJDO + O = ODA2DO + OH	7.0262E+06	1.611	-10.59
112	A2OJDO + O2 = ODA2DO + HO2	4.0910E+02	2.772	4.78

<sup>a</sup>The units of A factors and rate constants, k, are s<sup>-1</sup> for unimolecular reactions and cm<sup>3</sup> mol<sup>-1</sup> s<sup>-1</sup> for bimolecular reactions.  $E_A$  in kcal mol<sup>-1</sup>.



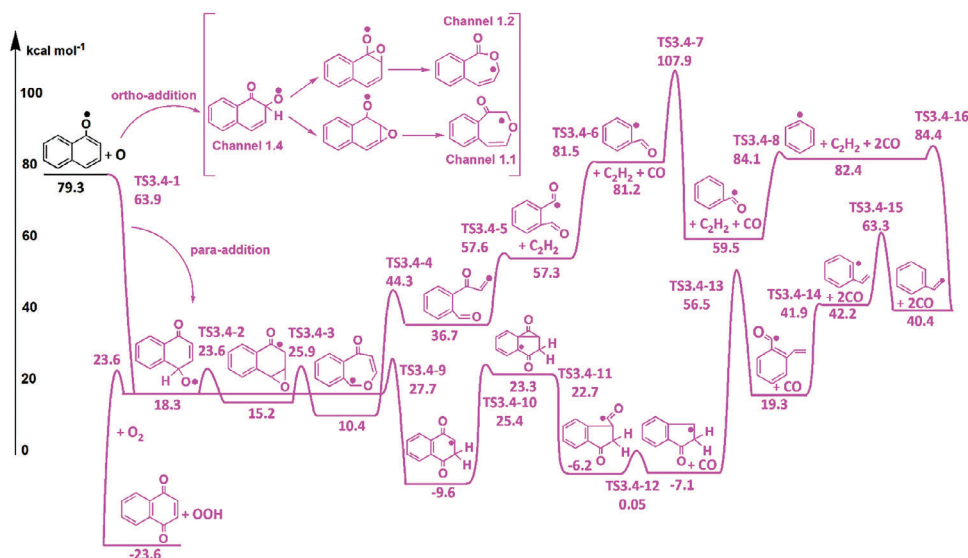


FIGURE 14 Channel 3.4: Oxidation of A2•DO to formation and further reactions of A2O•DO (APFD/6-311G(d,p) calculations).

as illustrated in Figures 5–14 are presented. Also, reactions of O<sub>2</sub> and O in the subsequent reactions are included (see Figures 10, 13, and 14).

In order to adjust the nomenclature to the CHEMKIN format, all radicals labelled in Section 3 by “•” are now identified with “J” in Table 1.

## 5 | SUMMARY AND CONCLUSIONS

The reaction of the 1-naphthyl radical C<sub>10</sub>H<sub>7</sub>• (A2•) with molecular and atomic oxygen, as part of the oxidation reactions of naphthalene up to the species C<sub>6</sub>H<sub>5</sub>•, CO and C<sub>2</sub>H<sub>2</sub>, is examined using ab-initio and DFT quantum chemistry calculations. The calculations were performed employing different computational methods, viz. three DFT (B3LYP, M06 and APFD) as well as CBS-QB3.

Enthalpies of formation of the species as well as transition state structures involved in the investigated reaction systems A2• + O<sub>2</sub> / A2• + O have been calculated. The kinetic parameters of each path are determined using chemical activation analysis based on canonical transition state theory calculations. Determination of the reaction rate coefficients for the different reactions enables a primary sight on the importance of the different reaction paths.

The primary attack of O<sub>2</sub> on the naphthyl radical leads to a peroxy radical C<sub>10</sub>H<sub>7</sub>OO• (A2OO•), which undergoes further propagation and/or chain branching reactions. The reaction of A2• with <sup>3</sup>O<sub>2</sub> opens a number of main consecutive reaction channels with new ones not currently considered in oxidation mechanisms. The reaction paths comprise important exothermic chain branching reactions and the formation of unsaturated oxygenated hydrocarbon

intermediates. The primary attack of O<sub>2</sub> at the A2• radical has a well depth of some 50 kcal mol<sup>-1</sup> while the six consecutive channels exhibit energy barriers below the energy of the A2• radical.

The investigated reactions could serve as part of a comprehensive mechanism for the oxidation of naphthalene. The principal result from this study is that the consecutive reactions of the A2• radical, viz. the channels conducting to a phenyl radical C<sub>6</sub>H<sub>5</sub>•, CO<sub>2</sub>, CO (which oxidized to CO<sub>2</sub>) and C<sub>2</sub>H<sub>2</sub> are by orders of magnitude faster than the activation of naphthalene by oxygen (A2 + O<sub>2</sub> → A2• + HO<sub>2</sub>). The results support the hypothesis that the pathways producing CO, phenyl and C<sub>2</sub>H<sub>2</sub> may constitute a repetitive reaction sequence for the successive diminution of six-membered rings also in larger polycyclic aromatic hydrocarbons.

## ACKNOWLEDGEMENTS

Open access funding enabled and organized by Projekt DEAL.

## DATA AVAILABILITY STATEMENT

The data that support the findings of this study are available from the corresponding author upon reasonable request.

## ORCID

Nadia Sebbar  <https://orcid.org/0000-0001-9832-2398>

## REFERENCES

1. Frenklach M, Wang H. Detailed modeling of soot particle nucleation and growth. *Proc Combust Inst.* 1991;23:1559.
2. Frenklach M. Reaction mechanism of soot formation in flames. *Phys Chem Chem Phys.* 2002;4:2028-2037.

3. Sebbar N, Bockhorn H, Trimis D. Oxidation of polycyclic aromatic hydrocarbons: evidence of similarities in thermochemical properties and reaction paths. *Combust Sci Technol.* 2023;195(14):3341-3356. doi:10.1080/00102202.2023.2239452
4. Sebbar N, Bockhorn H, Bozzelli JW. Thermodynamic properties of the species resulting from the phenyl radical with O<sub>2</sub> reaction system. *Int J Chem Kinet.* 2008;40:583-604.
5. Tokmakov IV, Kim G-S, Kislov VV, Mebel AM, Lin MC. The reaction of phenyl radical with molecular oxygen: a G2M study of the potential energy surface. *J Phys Chem A.* 2005;109:6114-6127.
6. Mebel AM, Landera A, Kaiser RI. Formation mechanisms of naphthalene and indene: from the interstellar medium to combustion flames. *J Phys Chem A.* 2017;121:901-926.
7. Chu TC, Smith MC, Yang J, Liu M, Green WH. Theoretical study on the HACA chemistry of naphthalenyl radicals and acetylene: the formation of C<sub>12</sub>H<sub>8</sub>, C<sub>14</sub>H<sub>8</sub>, and C<sub>14</sub>H<sub>10</sub> species. *Int J Chem Kinet.* 2020;52:752-768.
8. Parker DSN, Kaiser RI, Bandyopadhyay B, Kostko O, Troy TP, Ahmed M. Unexpected chemistry from the reaction of naphthyl and acetylene at combustion-like temperatures. *Angew Chem, Int Ed.* 2015;54:5421-5424.
9. Comandini A, Brezinsky K. Theoretical study of the Formation of naphthalene from the radical/ $\pi$ -bond addition between single-ring aromatic hydrocarbons. *J Phys Chem A.* 2011;115:5547.
10. Bunce NJ, Liu L, Zhu J, Lane DA. Reaction of naphthalene and its derivatives with hydroxyl radicals in the gas phase. *Environ Sci Technol.* 1997;31:2252-2259.
11. Sreekanth R, Prasanthkumar KP, Paul MMS, Aravind UK, Aravindakumar CT. Oxidation reactions of 1- and 2-naphthols: an experimental and theoretical study. *J Phys Chem A.* 2013;117:11261-11270.
12. Zhang Z, Lina L, Wang L. Atmospheric oxidation mechanism of naphthalene initiated by OH radical. A theoretical study. *Phys Chem Chem Phys.* 2012;14:2645-2650.
13. Shiroudi A, Deleuze MS. Theoretical study of the oxidation mechanisms of naphthalene initiated by hydroxyl radicals: the H abstraction pathway. *J Phys Chem A.* 2014;118:3625-3636.
14. Gnanaprakasam M, Sandhiya L, Senthilkumar K. A theoretical investigation on the mechanism and kinetics of the gasphase reaction of naphthalene with OH radical. *Theor Chem Acc.* 2017;136:131.
15. Kunioishi N, Touda M, Fukutani S. Computational study on the formation of five-membered rings in PAH through reaction with O<sub>2</sub>. *Combust Flame.* 2002;128(3):292-300.
16. Park J, Xu ZF, Lin MC. Kinetic study of the C<sub>10</sub>H<sub>7</sub> + O<sub>2</sub> reaction. *J Phys Chem A.* 2009;113:5348-5354.
17. Zhang F, Nicolle A, Xing L, Klippenstein SJ. Recombination of aromatic radicals with molecular oxygen. *Proc Combust Inst.* 2017;36:169-177.
18. Zhou C-W, Kislov VV, Mebel AM. Reaction mechanism of naphthyl radicals with molecular oxygen. 1. Theoretical study of the potential energy surface. *J Phys Chem A.* 2012;116:1571-1585.
19. Kislov VV, Singh RI, Edwards DE, Mebel AM, Frenklach M. Rate coefficients and product branching ratios for the oxidation of phenyl and naphthyl radicals: a theoretical RRKM-ME study. *Proc Combust Inst.* 2015;35:1861-1869.
20. Gaussian 16, Revision C.01, Frisch MJ, Trucks GW, Schlegel HB, et al. Gaussian, Inc., Wallingford CT, 2016.
21. Gaussian.com Expanding the limits of computational chemistry.
22. Zhao Y, Truhlar DG. The M06 suite of density functionals for main group thermo-chemistry, thermochemical kinetics, noncovalent interactions, excited states, and transition elements: two new functionals and systematic testing of four M06-class functionals and 12 other functionals. *Theor Chem Acc.* 2008;120:215-241.
23. Zhao Y, Truhlar DG. Applications and validations of the Minnesota density functionals. *Chem Phys Lett.* 2011;502:1-13.
24. Austin A, Petersson G, Frisch MJ, Dobek FJ, Scalmani G, Throssell K. A density functional with spherical atom dispersion terms. *J Chem Theory Comput.* 2012;8:4989.
25. Becke AD. Density-functional thermochemistry. III. The role of exact exchange. *J Chem Phys.* 1993;98:5648-5652.
26. Lee C, Yang W, Parr RG. Development of the Colic-Salvetti correlation-energy formula into a functional of the electron density. *Phys Rev B.* 1988;37:785-789.
27. Montgomery JA, Ochterski JW, Petersson GAA. Complete basis set model chemistry. IV. An improved atomic pair natural orbital method. *J Chem Phys.* 1994;101:5900-5909.
28. Montgomery Jr JA, Frisch MJ, Ochterski JW, Petersson GA. A complete basis set model chemistry. VI. Use of density functional geometries and frequencies. *J Chem Phys.* 1999;110:2822.
29. Montgomery Jr JA, Frisch MJ, Ochterski JW, Petersson GA. A complete basis set model chemistry. VII. Use of the minimum population localization method. *J Chem Phys.* 2000;112:6532.
30. Mebel AM, Diau EWG, Lin MC, Morokuma K. Ab initio and RRKM calculations for multichannel rate constants of the C<sub>2</sub>H<sub>3</sub> + O<sub>2</sub> reaction. *J Am Chem Soc.* 1996;118:9759.
31. Petersson GA, Malick DK, Wilson WG. Calibration and comparison of the Gaussian-2, complete basis set, and density functional methods for computational thermochemistry. *J Chem Phys.* 1998;109:10570.
32. Durant JL. Evaluation of transition state properties by density functional theory. *Chem Phys Lett.* 1996;256:595.
33. Byrd EFC, Sherril D, Head-Gordon M. The Theoretical prediction of molecular radical species: a systematic study of equilibrium geometries and harmonic vibrational Frequencies. *J Phys Chem A.* 2001;105:9736.
34. Sheng C. Ph.D. Dissertation. Department of Chemical Engineering, Chemistry and Environmental Science, New Jersey Institute of Technology; 2002.
35. Lay TH, Krasnoperov LN, Venanzi CA, Bozzelli JW. Ab initio study of  $\alpha$ -chlorinated ethyl hydroperoxides CH<sub>3</sub>CH<sub>2</sub>OOH, CH<sub>3</sub>CHClOOH, and CH<sub>3</sub>CCl<sub>2</sub>OOH: conformational analysis, internal rotation barriers, vibrational frequencies, and thermodynamic properties. *J Phys Chem.* 1996;100:8240-8249.
36. Sebbar N, Bozzelli JW, Bockhorn H, Trimis D. Pyrene + O<sub>2</sub>: primary reactions, reaction pathways, and influence of functional groups. Proc. of the 9th ECM, Lisboa, Portugal; 2019.
37. Tokmakov IV, Kim G-S, Kislov VV, Mebel AM, Lin MC. The reaction of phenyl radical with molecular oxygen: a G2M study of the potential energy surface. *J Phys Chem A.* 2005;109:6114-6127.
38. Sebbar N, Bockhorn H, Bozzelli JW. Thermochemistry and kinetics for 2-Butanone-3yl radical (CH<sub>3</sub>C(=O)CH<sub>2</sub>CH<sub>3</sub>) reactions with O<sub>2</sub>. *Z Phys Chem.* 2011;225:993-1018.

39. Sebbar N, Bockhorn H, Bozzelli JW. Thermochemistry and kinetics for 2-Butanone-1-yl radical ( $\text{CH}_2\cdot\text{C}(=\text{O})\text{CH}_2\text{CH}_3$ ) reactions with  $\text{O}_2$ . *J Phys Chem A*. 2014;118:21-37.
40. Sebbar N, Bozzelli JW, Trimis D, Bockhorn H. Thermochemistry and kinetics of the 2-butanone-4-yl  $\text{CH}_3\text{C}(=\text{O})\text{CH}_2\text{CH}_2\cdot + \text{O}_2$  reaction system. *Int J Chem Kinet*. 2001;51:541-562.
41. RMG – Reaction Mechanism Generator (mit.edu)
42. Sebbar N, Bockhorn H, Bozzelli JW. Thermochemistry and reaction paths in the oxidation reaction of benzoyl radical:  $\text{c}_6\text{H}_5\text{C}(=\text{O})\cdot$ . *J Phys Chem A*. 2011;115:11897-11914.
43. Morozov AN, Medvedkov IA, Azyazov VN, Mebel AM. Theoretical study of the phenoxy radical recombination with the O(3 P) atom, phenyl plus molecular oxygen revisited. *J Phys Chem A*. 2021;125:3965-3977.

## SUPPORTING INFORMATION

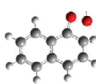
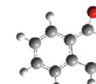
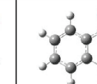
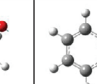

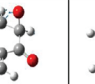
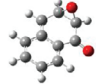
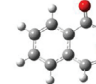
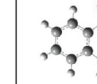
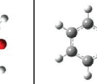
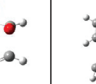
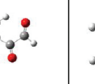
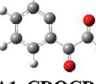
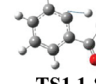

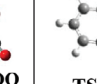
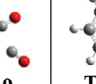
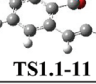

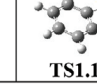
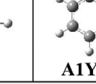
Additional supporting information can be found online in the Supporting Information section at the end of this article.

**How to cite this article:** Sebbar N, Bockhorn H, Trimis D. Oxidation of the 1-naphthyl radical  $\text{C}_{10}\text{H}_7\cdot$  with oxygen: Thermochemistry, kinetics, and possible reaction pathways. *Int J Chem Kinet*. 2023;1-23. <https://doi.org/10.1002/kin.21702>

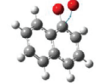
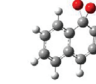
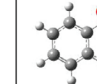
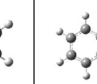
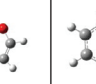
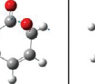
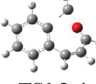
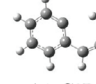
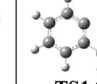
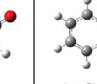
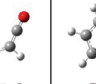
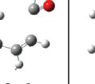
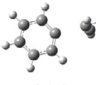
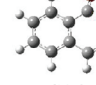
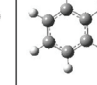
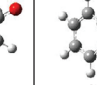
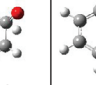
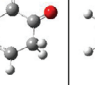
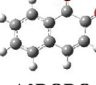
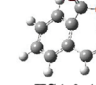
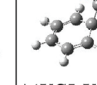
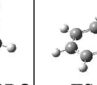
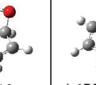
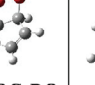

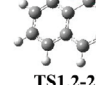
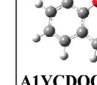
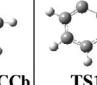
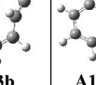
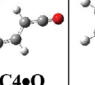

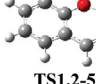
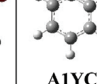
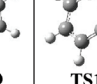
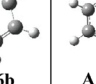
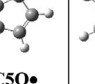
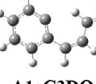
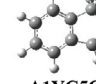
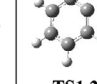
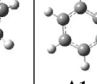
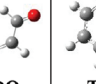
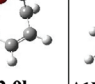
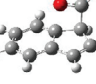
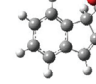
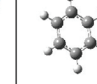
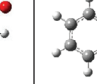
## APPENDIX

TABLE A Structures and nomenclature of intermediate species, transition states (TST), and products of channels 1 to 3.

**Channel 1.1:** Formation and further reactions of A2•YC2O2**Addition of the oxygen atom to the adjacent carbon atom**

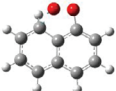
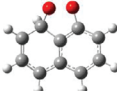
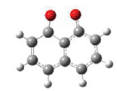
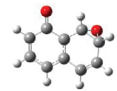
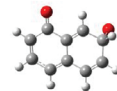
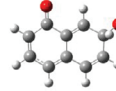
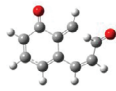
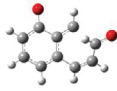
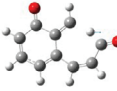
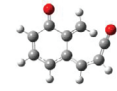
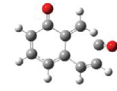
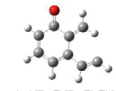
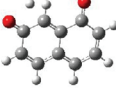
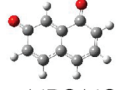
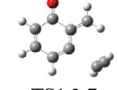
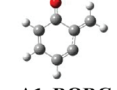
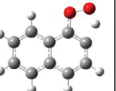
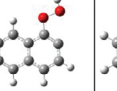


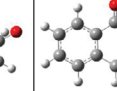
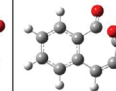
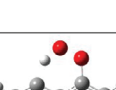
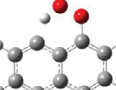
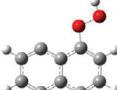
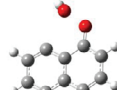
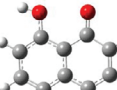
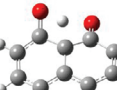
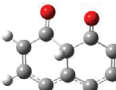
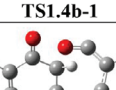
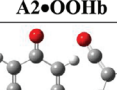
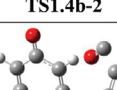
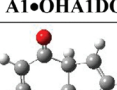
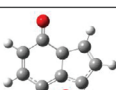
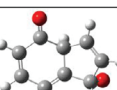
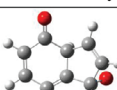
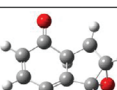
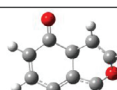
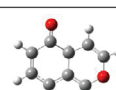
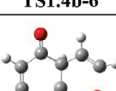
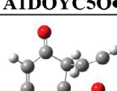
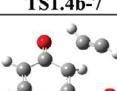
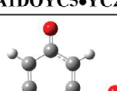
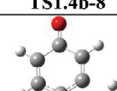
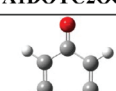
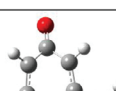
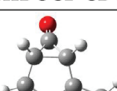
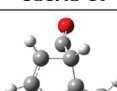
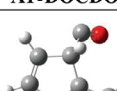
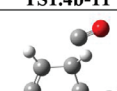
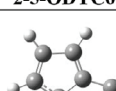
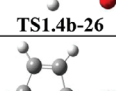
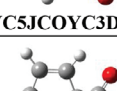
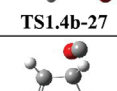
Channel 1.1: Formation and further reactions of A2•YC2O2 Addition of the oxygen atom to the adjacent carbon atom					
 TS1.1-1	 A2•YC2O2	 TS1.1-2	 A2O•CDO	 TS1.1-3	 TS1.1-4
 A2DOYC2OC•	 TS1.1-5	 A1YC2OC•CDO	 TS1.1-6	 A1CC•CDOCDO	 TS1.1-7
 A1•CDOCDO	 TS1.1-8	 A1CDOC•DO	 TS1.1-9	 TS1.1-10	
 TS1.1-11	 A1YC5O•CO	 TS1.1-12	 A1YC5DO		

**Channel 1.2:** Formation and further reactions of A2•YCO2  
Ipsso addition of the oxygen atom to the ring

 TS1.2-1	 A2•YCO2	 TS1.2-2	 A1YCD0OC•CC	 TS1.2-3	 A1C3OC•DO
 TS1.2-4	 A1•C3DO	 TS1.2-5	 A1C2C•DO	 TS1.2-6	 A1CDC•
 TS1.2-7	 TS1.2-8	 A1OD A1O•	 TS1.2-9	 A2•DODO	 TS1.2-10
 A2DODO	 TS1.2-11	 A1YC5•YC3ODO	 TS1.2-12	 A1YC5OC•DO	 TS1.2-13
 A1YC5•	 TS1.2-2b	 A1YCD0OC•CCb	 TS1.2-3b	 A1DOC4•O	 TS1.2-4b
 A1YC5•OCDO	 TS1.2-5b	 A1YC5•O	 TS1.2-6b	 A1YC5O•	 TS1.2-7b
 A1•C3DO	 A1YC5O•	 TS1.2-8b	 A1•C3DO	 TS1.2-9b	 A1YC5•YC3ODOb
 TS1.2-10b	 A1YC5CO2•	 TS1.2-11b	 A1YC5•		

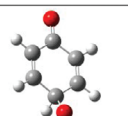
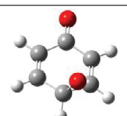
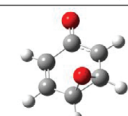
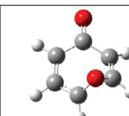
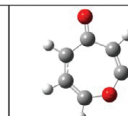
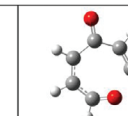
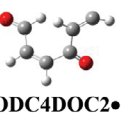
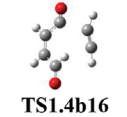

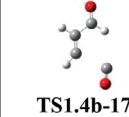
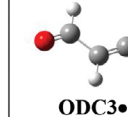
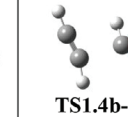
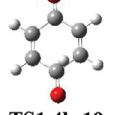

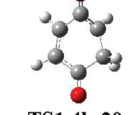
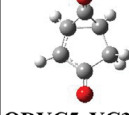
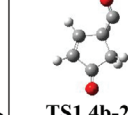
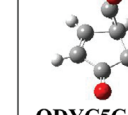
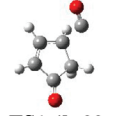
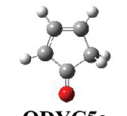
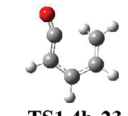

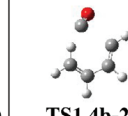
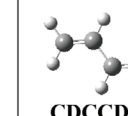
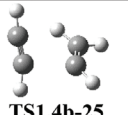
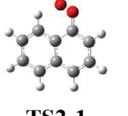
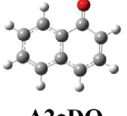
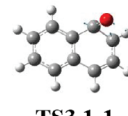
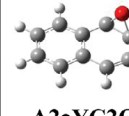
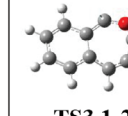
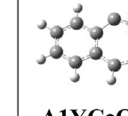
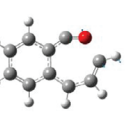
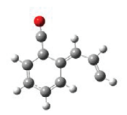
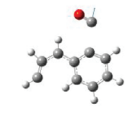
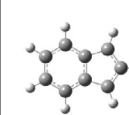
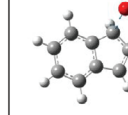
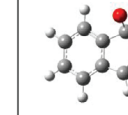
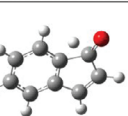
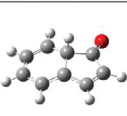
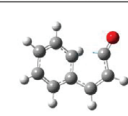
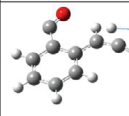
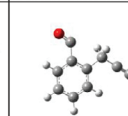
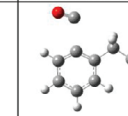
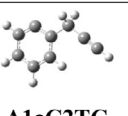
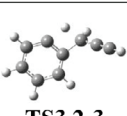
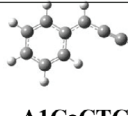
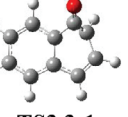
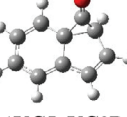
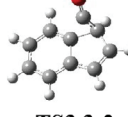
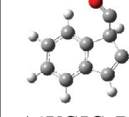
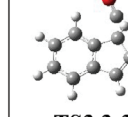
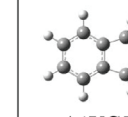
(Continues)

TABLE A (Continued)

Channel 1.3: Formation and further reactions of A2•YC3O2					
Addition of the oxygen atom to the adjacent ring					
					
TS1.3-1	A2•YC3O2	TS1.3-2	A1•DOA1YC2O	TS1.3-3	A1DOA1O•
					
TS1.3-4	A1DODC•C3DO	TS1.3-5	RC3•DO	TS1.3-6	A1DODCC2•
					
TS1.3-8	o-A1DOA1O	TS1.3-7	A1•DODC		
Channel 1.4: Formation and further reactions of A2•OOH					
Abstraction of hydrogen atom from the same ring					
					
TS1.4a-1	A2•OOHa	TS1.4a-2	A1A1•OHDO	TS1.4a-3	A1A1O•DO
					
Abstraction of hydrogen atom from the adjacent ring					
					
TS1.4b-1	A2•OOHb	TS1.4b-2	A1•OHA1DO	TS1.4b-3	A1DOA1•DO
					
TS1.4b-4	A1•DOC4DO	TS1.4b-5	A1DOYC5•		
Addition of an oxygen atom to A1DOYC5•					
					
TS1.4b-6	A1DOYC5O•	TS1.4b-7	A1DOYC5•YC2O	TS1.4b-8	A1DOYC2OC•
					
TS1.4b-9	A1DOC2•CDO	TS1.4b-10	A1•DOCDO	TS1.4b-11	2-5-ODYC6•
					
TS1.4b-26	YC5JCOYC3DO	TS1.4b-27	YC5COCJDO	TS1.4b-28	YC5JCDO
					
TS1.4b-29	YC5CJDO	TS1.4b-30			

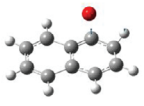
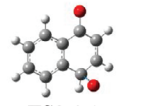
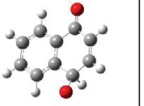
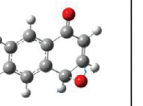
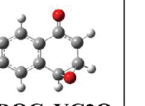
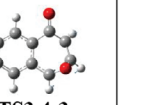
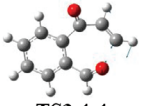
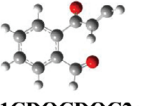
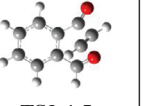

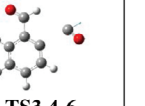
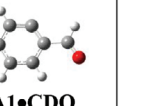
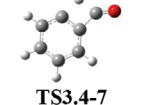
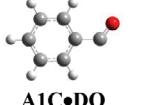
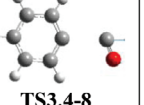

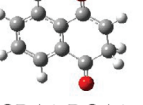
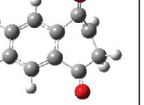
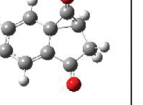
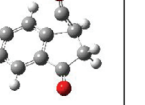
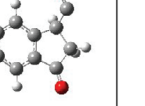
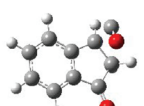

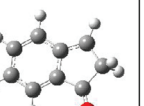
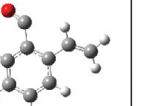
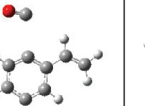
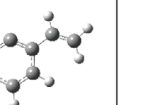
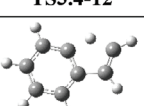
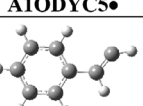
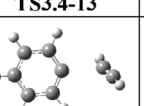
(Continues)

TABLE A (Continued)

Addition of an oxygen atom to 2-5-ODYC6•					
 25ODYC6O•	 TS1.4b-13	 25ODYC6•YC2O	 TS1.4b-14	 25ODYC6•O	 TS1.4b-15
 ODC4DOC2•	 TS1.4b16	 ODC3C•DO	 TS1.4b-17	 ODC3•	 TS1.4b-18
 TS1.4b-19	 ODA1•DO	 TS1.4b-20	 ODYC5•YC3DO	 TS1.4b-21	 ODYC5C•DO
 TS1.4b-22	 ODYC5•	 TS1.4b-23	 CDCCDCC•DO	 TS1.4b-24	 CDCCDC•
 TS1.4b-25					
Channel 2, 3.1, 3.2 and 3.3: Formation and further reactions of A2•DO O—O bond cleavage and further reactions					
 TS2-1	 A2•DO	 TS3.1-1	 A2•YC2O	 TS3.1-2	 A1YC•OC3
 TS3.1-3	 A1DCDOC3•	 TS3.1-4	 A1YC5•	 TS3.1-5	 A1YC5O•
 TS3.1-6	 A1•YC5DO	 TS3.1-7	 TS3.2-1	 A1C•OCCTC	 TS3.2-2
 A1•C2TC	 TS3.2-3	 A1C•CTC			
 TS3.3-1	 A1YC5•YC3DO	 TS3.3-2	 A1YC5C•DO	 TS3.3-3	 A1YC5•

(Continues)

TABLE A (Continued)

<b>Channel 3.4: Formation and further reactions of A2O•DO</b> <b>Addition of an oxygen atom on C<sub>10</sub>H<sub>7</sub>O• = A2•DO + O = A2O•DO</b>					
 TS3.4-1	 TS3.4-1	 A2O•DO	 TS3.4-2	 A2DOC•YC2O	 TS3.4-3
 TS3.4-4	 A1CDOCOC2•	 TS3.4-5	 ODCA1C•DO	 TS3.4-6	 A1•CDO
 TS3.4-7	 A1C•DO	 TS3.4-8			
 TS3.4-9	 ODA1•DOA1	 TS3.4-10	 A1OYC5•YC3DO	 TS3.4-11	 A1ODYC5C•DO
 TS3.4-12	 A1ODYC5•	 TS3.4-13	 A1C•OCDC	 TS3.4-14	 A1•CDC
 TS3.4-15	 A1CDC•	 TS3.4-16			